ISSN 1843 - 7583

North University of Baia Mare Carpathian Journal of Electrical Engineering Volume 4, Number 1, 2010

Volume 4, Number 1, 2010

North University of Baia Mare
Faculty of Engineering
Electrical Engineering Department

Carpathian Journal of Electrical Engineering

NORDTECH PUBLISHER

NORTH UNIVERSITY of BAIA MARE
FACULTY of ENGINEERING
ELECTRICAL ENGINEERING DEPARTMENT

RO-430083, Baia Mare, Maramureş county, dr. Victor Babeş street, no. 62A,
phone: +40 (0) 362-401256 **fax:** +40 (0) 262-276153
http://www.ubm.ro

Carpathian Journal of Electrical Engineering

Volume 4, Number 1, 2010
ISSN 1843 – 7583

http://cee.ubm.ro/cjee.html

CONTENTS

HIGH FREQUENCY ELECTROMAGNETIC PROCESSES IN INDUCTION MOTORS SUPPLIED FROM PWM INVERTERS

Ioan **ȚILEA**
North University of Baia Mare

Key words: ***electromagnetic interference, inverter, induction motor***
Abstract: *The paper presents the electromagnetic interference between induction motors and inverters when at high frequency electromagnetic process appears in induction motors having a parallel resonant effect because of parasitic capacitive coupling between windings and ground, using a numerical model in simulink and a high frequency induction motor equivalent circuit model this effect is shown.*

1. INTRODUCTION

In modern PWM variable frequency AC motor drive the switching frequency is very high, up to 200 kHz. The high frequency components of the inverter output voltage involves electromagnetic interference problems, such as resonant parallel effect, due to the stray capacitance between windings and ground. The output voltage of the inverter is generated as a pulse string; the resultant current is modified substantially by the motor inductance and consists basically of a sine wave at the fundamental frequency [1].

When supplying AC motors with high switching frequency because of the resonant effect the motor inductance is modify and the current no longer consists of a sin wave but becomes more like the inverter output voltage thus the *di/dt* greatly increases.

In order to predict the conducted electromagnetic interference, high frequency induction motor equivalent circuit will be used.

2. THE BASIC MODELS

The simulink model of the investigated system in shown in fig.1, it composes of a 400 V IGBT inverter supplying a 7.5 kW induction motor.

The induction motor high frequency equivalent model have been proposed and deeply analyzed in [2], and the proposed equivalent three phase circuit is shown in fig.2. In [2] it has been verified that the stator winding phase resistance and the turn-to-turn distributed capacitive coupling can be neglected in the high frequency motor model.

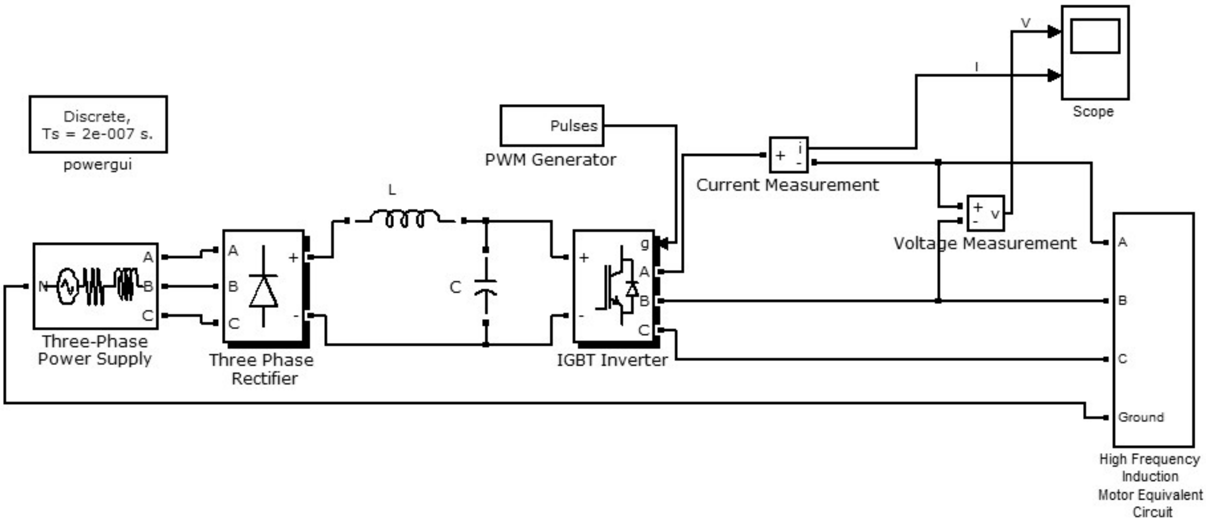

Fig. 1 – The investigated drive system

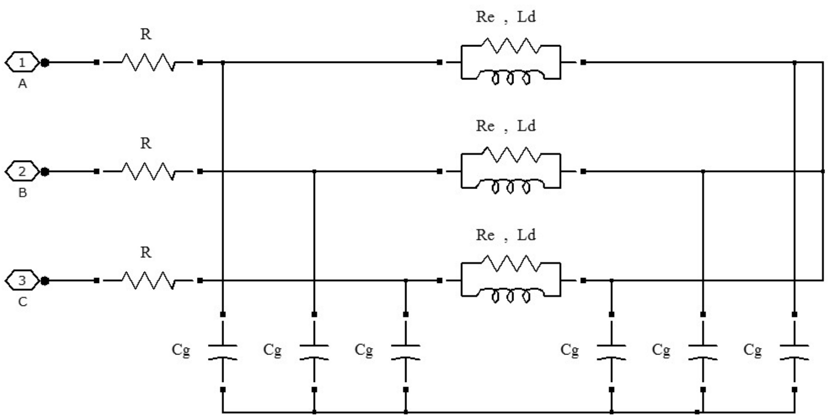

Fig. 2 – The selected equivalent circuit of the induction motor

The parameters considered in fig. 2 are:

R - winding resistance;

Ld- phase leakage inductance;

Re- resistance representing eddy currents inside the magnetic core and the frame;

Cg- capacitance representing the winding to ground distributed capacitance;

3. SIMULATION RESULTS

The simulations were made in simulink using the models in fig.1 and fig. 2; the fundamental frequency of the inverter has been keep at a constant 50 Hz only the switching frequency is modify.

The values for the parameters considered in fig. 2 were obtained from [2], for a 7.5 kW induction motor:

Cg= 0.953[nF];

Ld= 12.5[mH];

Re= 7.54[kΩ];

The first simulation was carried out at a 2.5 kHz switching frequency, representing a low switching frequency thyristor inverter; the results are shown in fig. 3.

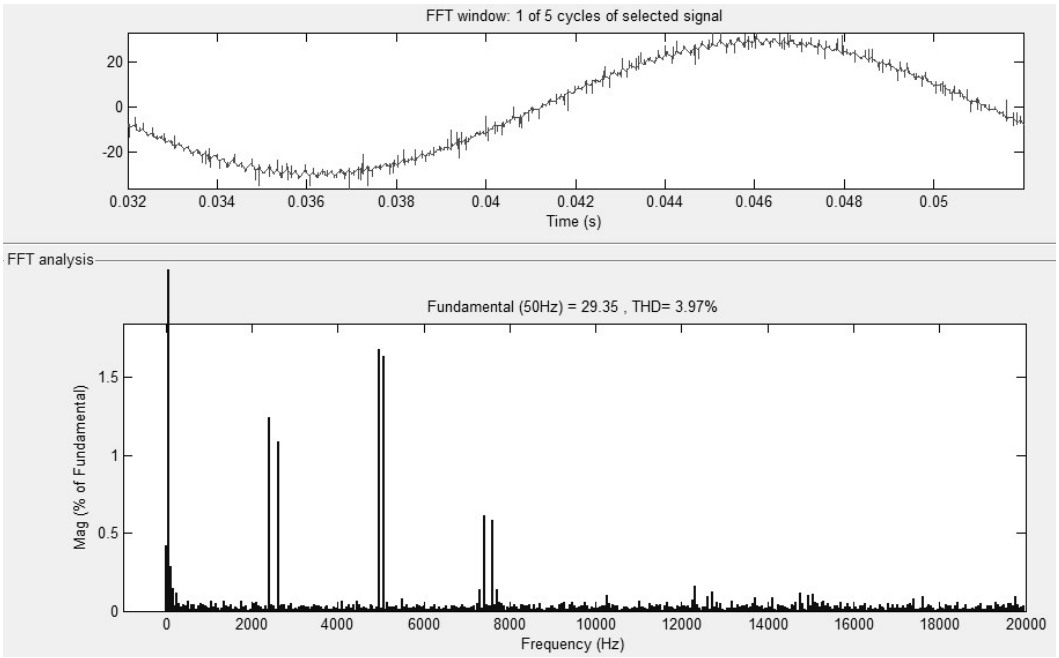

Fig. 3 – FFT result at 2.5 kHz switching frequency

Using the FFT (Fast Fourier Transform) Analysis Tool from simulink software, the waveform and harmonic content of the inverter output current is presented in fig. 3.

The output current waveform of the inverter is modified substantially by the motor inductance consisting of a sine wave at the fundamental frequency; because of the motor inductance the harmonic content of the output current is very low.

In fig. 4 the switching frequency is increased to 25 kHz, representing most transistor inverters switching frequency.

It can be seen that the motor inductance did not substantially modified the output current waveform of the inverter, meaning that the motor inductance has decreased; because the winding inductance and the winding to ground parasitic capacitive the motor becoming a parallel LC circuit.

In fig. 5 the switching frequency is increased to 200 kHz, representing a modern IGBT inverter [3]. The motor inductance has decreased even more because of the parallel resonant effect that cancels the motor inductance accentuated by the high switching frequency.

The harmonic content of the inverter output current is very high especially in high frequency harmonics with a THD (Total Harmonic Distortion) of 27%.

In all of the tree simulation results, represented in fig.3, fig.4, fig.5; only the switching frequency was modify (2.5 kHz, 25 kHz and 200 kHz), the fundamental frequency was constant at 50 Hz.

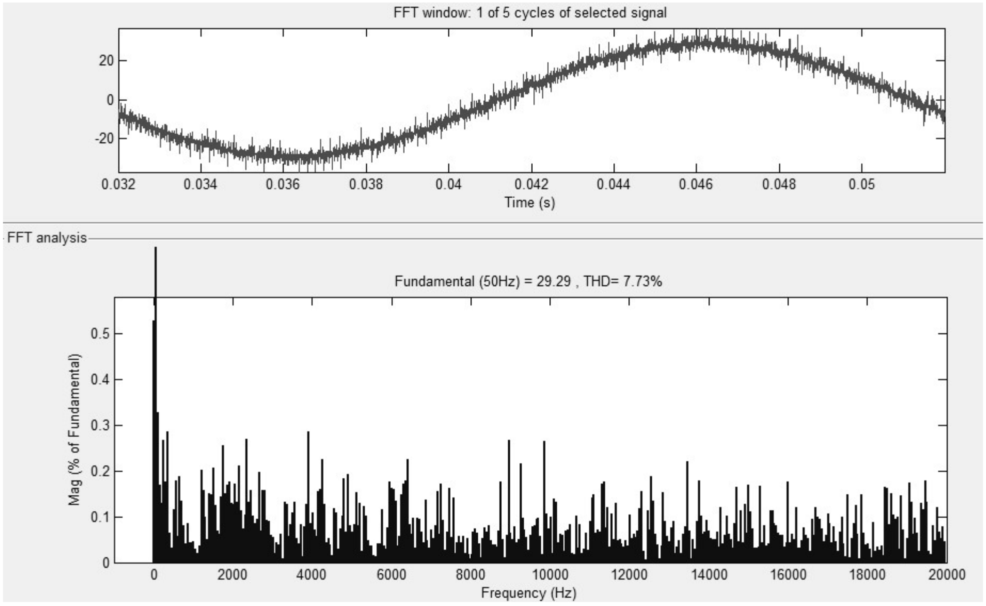

Fig. 4 – FFT result at 25 kHz switching frequency

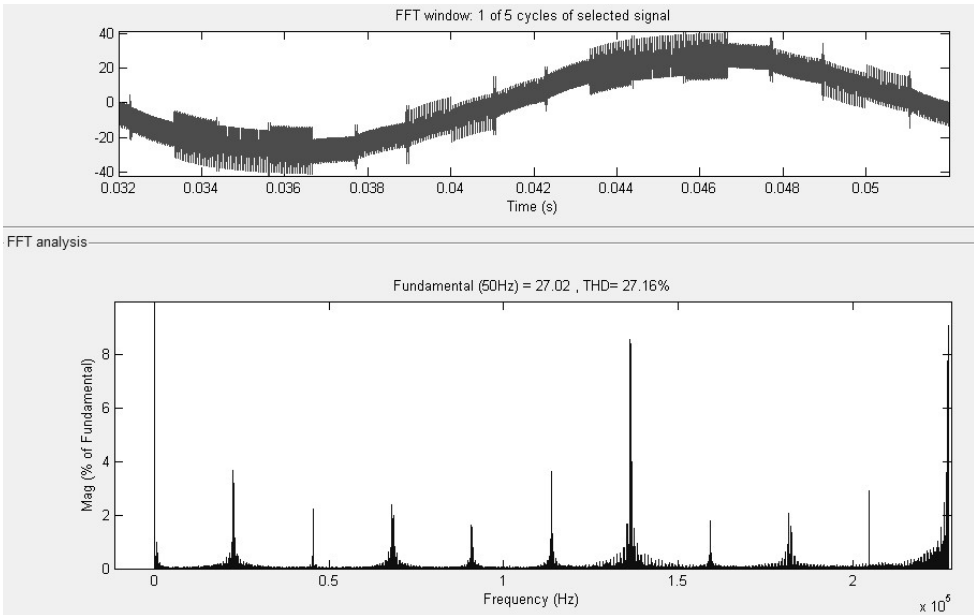

Fig. 5 – FFT result at 200 kHz switching frequency

4. CONCLUSION

At high switching frequencies the inverter power losses dramatically decreases so there is an interest in making inverters that can work at high switching frequencies. Using a power filter will minimize the effect of the high switching frequency but some application such as vector control used in variable speed drives cannot work using output power filters.

High switching frequencies create electromagnetic interference problems between inverter and motor in the form of resonant effects that cancels out the motor inductance, increasing the *di/dt* output current of the inverter producing even more electromagnetic interference along inverter-motor cable path.

REFERENCES

1. **GAMBICA/REMA Technical Guide**, *Variable speed drives and motors*, Technical Report No.2, 2002.
2. **A. Boglietti, A. Cavagnino, M. Lazzari**, *Experimental high frequency parameter identification of AC electrical motors,* IEEE Xplore, 2005.
3. **T. Friedli, S. D. Round, D. Hassler, J. W. Kolar**, *Design and performance of a 200 kHz All-SiC JFET Current Source Converter,* Industry Applications Society Annual Meeting, 2008.
4. **J. Luszcz, K. Iwan,** *Conducted EMI propagation in inverter-fed AC motors,* Electrical Power quality and Utilisation, Magazine Vol. II, No.1, 2006.
5. **S. Bartos, I. Dolezel, J. Necesany, J. Skramlik, V. Valouch**, *Theoretical and experimental investigation of parasitic effects in induction motors drives supplied from semiconductor inverters,* Acta Electrotehnica et Informatica, Vol. 8, No. 4, 2008.

ON DISTRIBUTED MODEL PREDICTIVE CONTROL FOR LOAD FREQUENCY PROBLEM

Cristinel **COSTEA**
North University from Baia Mare, Electric Department, ccostea@ubm.ro

Key words: Distributed Control, Load Frequency Control, Multi-Agent Systems

Abstract*: The paper discribe a multi-agent application in power systems for the problem of Load Frequency Control. The connections between subsystems are treated by each controller agent as a set of disturbance signals. Each area maintain the tie-lines power flow to specified values,based on communication between neighboring agents.*

1. INTRODUCTION

One of the most implemented advanced control techniques in last decade in the process industries [1] is Model Predictive Control (MPC), and its popularity is due to the versatility in coping with constraints. The main concept of MPC is to use a model of the plant to predict the future evolution of the system and is based on the idea of finite receding horizon, emulating infinite horizon optimal control algorithms.

Using a model of the system to be controlled, at each sample period *t* an optimal control problem is solved with the aid of constrained numerical optimization methods. Following this, only the first part of the solution is implemented for the duration of the sample period. Due to model uncertainty and disturbances, the actual output trajectory may deviate from the predicted trajectory, thus a measurement of the actual output at the next sample instant $t + 1$ is taken, and the optimal control problem is updated with the new measurement. This process of measuring, solving a constrained optimization problem and implementing only the first part of the optimal control sequence is repeated at future sample instants, and in this way a feedback control law is produced. A thorough survey on the subject is [2].

From an algorithmic perspective, most MPC implementations result in the requirement to solve, at each sample instant, a quadratic program (QP) :

$$\min_x \frac{1}{2} x^T H x + f^T x, \qquad s.t. \begin{cases} A \cdot x \leq b \\ A_{eq} x = b_{eq} \\ LB \leq x \leq UB \end{cases} \tag{1}$$

This is a centralized approach that is considered impractical for the control problem of large-scale systems (such as power networks), when the optimization problem is too big for real time computation. The solution may be to decompose the problem into a set of smaller subproblems and the overall system into appropriately subsystems with distinct MPC controllers for each subsystem.

The new method of distributed MPC can be solved in a parallel manner if the controllers are well coordinated; we intend to realize this by a particular communication among the agents and not through a centralized supervisor. Thus, each subsystem problem will be solved by an individual controller agent using local information and collaborating to other agents to achieve global decisions.

Multi-agent systems (MAS) paradigm has matured during the last decade and effective applications have been used; in MAS tasks are deploy by interacting entities (abstraction objects named *agents*), capable of autonomous actions in its environment; agents cooperates with each other, but each agent has incomplete information or capabilities for solving the problem (has a limited viewpoint); there is no system global control, data are decentralized and computation is asynchronous [3].

In industrial application agent technology can be use in process automation functions where the tasks require cooperative distributed problem solving. Typical applications refer to cooperative robots, sensor networks, traffic control, electronic markets. MAS can be considered "self-organized systems" as they tend to find the best solution for their problems without external intervention. Multi-agent technologies can be applied also, in a variety of applications related to power system, such as disturbance diagnosis, restoration, secondary voltage control or power system visualization [4].

2. MULTI-AGENT MODEL PREDICTIVE CONTROL

We will consider a network that is partitioned into n subnetworks and each subsystem model is represented as a discrete, linear time-invariant (LTI) model of the form (3)

$$\begin{cases} x_i(k+1) = A_i x(k) + B_i u_i(k) + E_i d_i(k) + H_i w_i(k) \\ y_i(k) = C_i x(k) \end{cases} \tag{2}$$

where at time k for subsystem i, $x_i(k) \in \mathbb{R}^{n_{x_i}}$ are local states, $u_i(k) \in \mathbb{R}^{n_{u_i}}$ are the local inputs, $d_i(k)$ are the local known perturbation, $y_i(k) \in \mathbb{R}^{n_{y_i}}$ are the local outputs and $w_i(k)$ are external influences due to interconnections between subsystems.

For each subsystem the controller will be implemented by a software agent; in each step k the agent compute the next command u_k solving an optimization problem (4) by collaboration with other similar agents.

$$J_{i,k} = \frac{1}{2}\sum_{p=0}^{N-1}\left[\left\|x_{k+p+1}\right\|_{Q_x}^2 + \left\|\Delta u_{k+p}\right\|_{Q_u}^2\right] \tag{3}$$

The expression of objective function from equation (4) can be expanded in order to reformulate the MPC problem such as a quadratic programming (QP) problem for which solvers are easy to find.

Just for simplicity will consider in next equations a prediction horizon N=3

$$J_i = \frac{1}{2}\sum_{k=0}^{N-1}\left[\|Ax_k + Bu_k + Hw_k\|_{Q_x}^2 + \|u_k - u_{k-1}\|_{Q_u}^2\right] =$$
$$= \frac{1}{2}\left[\|Ax_0 + Bu_0 + Hw_0\|_{Q_x}^2 + \|A^2x_0 + ABu_0 + AHw_0 + Bu_1 + Hw_1\|_{Q_x}^2 + \right.$$
$$+\|A^3x_0 + A^2Bu_0 + A^2Hw_0 + Bu_2 + Hw_2\|_{Q_x}^2 +$$
$$\left. +\|u_0 - u_{-1}\|_{Q_u}^2 + \|u_1 - u_0\|_{Q_u}^2 + \|u_2 - u_1\|_{Q_u}^2\right]$$

$$= \frac{1}{2}\left(\begin{bmatrix} A \\ A^2 \\ A^3 \end{bmatrix} x_0 + \begin{bmatrix} B & 0 & 0 & \vdots & H & 0 & 0 \\ AB & B & 0 & \vdots & AH & H & 0 \\ A^2B & AB & B & \vdots & A^2H & AH & H \end{bmatrix}\begin{bmatrix} u_0 \\ u_1 \\ u_2 \\ w_0 \\ w_1 \\ w_2 \end{bmatrix}\right)^T \cdot Q_x\left(\cdots\right)$$

$$+\frac{1}{2}\begin{bmatrix} u_0 \\ u_1 \\ u_2 \\ w_0 \\ w_1 \\ w_2 \end{bmatrix}^T \begin{bmatrix} 2Q_u & -Q_u & 0 & \vdots & \\ -Q_u & 2Q_u & -Q_u & \vdots & 0 \\ 0 & -2Q_u & +Q_u & \vdots & \\ \cdots & \cdots & \cdots & \vdots & \cdots \\ & 0 & & \vdots & 0 \end{bmatrix}\begin{bmatrix} u_0 \\ u_1 \\ u_2 \\ w_0 \\ w_1 \\ w_2 \end{bmatrix} + [-Q_u \cdot u_{-1}] \cdot u_0 \tag{4}$$

and with following notations

$$\hat{A} = \begin{bmatrix} A^1 \\ A^2 \\ A^3 \end{bmatrix}, \quad \hat{B} = \begin{bmatrix} B & 0 & 0 & . & H & 0 & 0 \\ AB & B & 0 & . & AH & H & 0 \\ A^2B & AB & B & . & A^2H & AH & H \end{bmatrix},$$

$$Z = \begin{bmatrix} u_0 \\ u_1 \\ u_2 \\ w_0 \\ w_1 \\ w_2 \end{bmatrix}, \quad H_u = \begin{bmatrix} 2Q_u & -Q_u & 0 & \vdots & \\ -Q_u & 2Q_u & -Q & \vdots & \\ 0 & -2Q & +Q & \vdots & 0 \\ \cdots & \cdots & \cdots & \vdots & \cdots \\ & 0 & & 0 & \end{bmatrix}, \tag{5}$$

The weight matrix Q_u, Q_u from (3) is given by

$$Q_u = \begin{bmatrix} q_u & 0 & \cdots & 0 \\ 0 & q_u & \cdots & 0 \\ \vdots & \vdots & \ddots & \vdots \\ 0 & 0 & \cdots & q_u \end{bmatrix}, Q_x = \begin{bmatrix} q_x & 0 & \cdots & 0 \\ 0 & q_x & \cdots & 0 \\ \vdots & \vdots & \ddots & \vdots \\ 0 & 0 & \cdots & q_x \end{bmatrix} \tag{6}$$

and the objective function of agent i in step k can be written now as a QP problem:

$$J_{i,k} = \frac{1}{2} \cdot Z^T \cdot \tilde{H} \cdot Z + f^T \cdot Z \tag{7}$$

The MPC problem in this form is echivalent to (4) for which standard and efficient codes exist, many suppliers of MPC writing their own solvers [5]. The QP solver shipped together with Matlab (*quadprog*) computes the answer with ten degrees of freedom or more in well under a second, but generally are considered rather slow in terms of computational speed; however Matlab provides a unified interface to other solvers.

The objective function (3) or (7) uses a quadratic cost function subject to the constraints imposed on the manipulated variables as well as state or/and output variables, expressing as a variable rate change or to keep the variable within certain bounds. According to system equation (2), constraints can be formulated:

$$\begin{cases} y_i^{min} \le y(k+i|k) \le y_i^{max} \\ u_i^{min} \le u(k+p-1|k) \le u_i^{max} \\ \Delta u_i^{min} \le \Delta u(k+p-1|k) \le \Delta u_i^{max} \end{cases} \tag{8}$$

but it can be easly reformulated in term of equation (7).

The communication between agents can improve the predictions about the future evolutions of interconnections variables. The observations in [6] suggest that information exchange between neighboring agents can have a beneficial effect in stability, when it leads to reduced prediction mismatch. As each system converges to its equilibrium, predictions on the behavior of neighbors should get more and more accurate to satisfy the stability condition.

Each of the agents in the system can use MPC and through an iterative scheme determine following actions, performing in parallel:

1) At sampling time instant k, agent i make a measurement of the current state of the subsystem x_k^i, send to and receive information from other neighboring agents.
2) Determine the best future behavior of local system according to a specified local objective, solving an optimization problem over a certain horizon. During this optimization there may be also communication with other agents.
3) Implement the first input u_k^i of found actions until the next step.
4) Move horizon to the next sampling time. Move on to the next decision step.

3. MULTI-AREA POWER SYSTEM MODEL

The frequency is one of the main variables characterizing the power systems. The purpose of load-frequency control (LFC) is to keep power generation equal to power consumption under consumption disturbances, such that the frequency is maintained close to a nominal frequency. LFC is becoming much more significant today due to deregulation of power systems, and in last years a number of decentralized control strategies has been developed for load-frequency control [7].

In a distributed manner, we consider more interconnected power subsystems where each area must contribute to absorb any load change such that frequency does not deviate and also, must maintain the tie-line power flow to its pre-specified value. If each considered area is supervised by an controller agent, the agents have to obtain agreement with other agents on power flowing over lines between subnetworks in order to be able to perform adequate local frequency control.

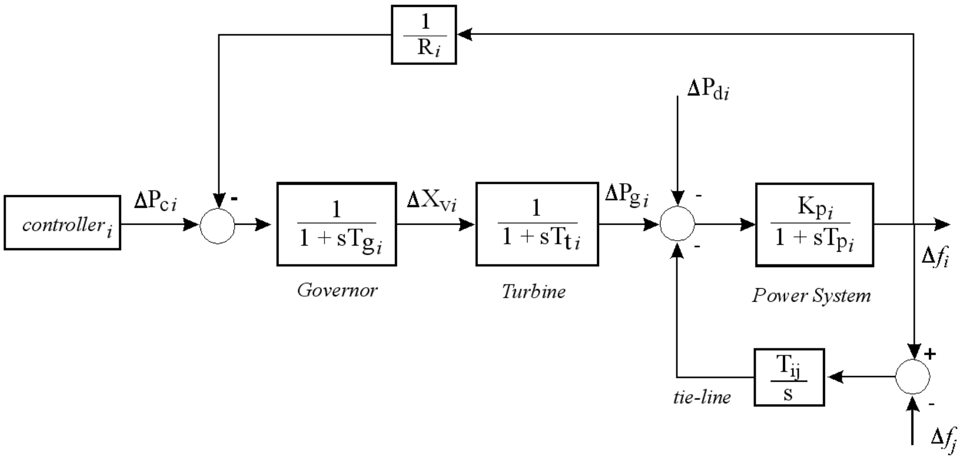

Fig.1 – Diagram for the subsystem i of multi-area system

Models for electric power systems are generally nonlinear. However, for load frequency control, the linearized model is generally used to design control schemes. Similar to [7][8][9], Fig. 1 shows a block diagram for the *i*th subsystem of a multi-area power system.

The notations used in the dynamic model description of the *i*th area power subsystem $i \in \{1,..,n\}$ are as follows:

Δf_i incremental change in frequency (Hz)

$\Delta\Delta\delta_i$ change in rotor angle

ΔP_{gi} incremental change in generator output (p.u. MW)

ΔX_{vi} incremental change in governor valve position (p.u. MW)

ΔP_{ci} incremental change in integral control

ΔP_{ti} incremental change in the tie line power (p.u. MW)

ΔP_{di} load disturbance (p.u. MW)
T_{gi} governor time constant (s)
T_{ti} turbine time constant (s)
T_{pi} plant model time constant (s)
K_{pi} plant gain for ith area subsystem
R_i speed regulation due to governor action (Hz /p.u. MW)

The state variable equations from block diagram are derived as follows [8],[9]:

$$\Delta\dot{\delta}_i(t) = 2\pi\Delta f_i \tag{9}$$

The differential equation for the power system:

$$\Delta\dot{f}_i(t) = -\frac{1}{T_{pi}}\cdot\Delta f_i + \frac{K_{pi}}{T_{pi}}[-\Delta P_{tie} - \Delta P_{di} + \Delta P_{gi}] \tag{10}$$

$$\Delta\dot{P}_{gi}(t) = -\frac{1}{T_{ti}}\cdot\Delta P_{gi} + \frac{1}{T_{ti}}\cdot\Delta x_{vi} \tag{11}$$

The differential equation for the speed governor :

$$\Delta\dot{x}_{vi}(t) = -\frac{1}{T_{gi}}\cdot\Delta x_{vi} - \frac{1}{T_{gi}\cdot R_i}\cdot\Delta f_i + \frac{1}{T_{gi}}\cdot\Delta P_{ci} \tag{12}$$

$$\Delta\dot{P}_{tie}(t) = 2\pi\sum_{j\neq i} T_{ij}(\Delta f_i - \Delta f_j) \tag{13}$$

With state space equation, similar to (2):

$$\begin{bmatrix}\Delta\dot{\delta}_i\\ \Delta\dot{f}_i\\ \Delta\dot{P}_{gi}\\ \Delta\dot{X}_{vi}\\ \Delta\dot{P}_{di}\\ \Delta\dot{\delta}_j\end{bmatrix} = \begin{bmatrix}0 & 2\pi & 0 & 0 & 0 & 0\\ -\frac{K_{pi}}{T_{pi}}T_{ij} & -\frac{1}{T_{pi}} & \frac{K_{pi}}{T_{pi}} & 0 & \frac{-K_{pi}}{T_{pi}} & \frac{K_{pi}}{T_{pi}}T_{ij}\\ 0 & 0 & -\frac{1}{T_t} & \frac{1}{T_t} & 0 & 0\\ 0 & -\frac{1}{T_{gi}R_i} & 0 & -\frac{1}{T_{gi}} & 0 & 0\\ 0 & 0 & 0 & 0 & 0 & 0\\ 0 & 0 & 0 & 0 & 0 & 0\end{bmatrix}\begin{bmatrix}\Delta\delta_i\\ \Delta f_i\\ \Delta P_{gi}\\ \Delta X_{vi}\\ \Delta P_{di}\\ \Delta\delta_j\end{bmatrix} + \begin{bmatrix}0\\0\\0\\ \frac{1}{T_{gi}}\\0\\0\end{bmatrix}\Delta P_{ci} \tag{14}$$

4. SIMULATIONS

The proposed adaptive control scheme is applied to the load frequency control problem of a two subsystems. The system is simulated in discrete time steps using MATLAB programming language.

The parameters of the power systems are such that: $T_p=20,\ T_t=0.5,\ T_g=0.4,\ K_p=100,\ R=2.7$. At first, with Q_u selected randomly, although the outputs y_1, y_2 were stable, the interconnections variables w_1, w_2 (in fact rotor angles – first column in Fig.2) was unstable. After several simulations, we can achieve better results for $q_u=100$. Two independent perturbations are considered in each subsystem at time 3s and 7s respectively; load disturbance parameter: $\Delta P_{D,1}$= 0.17 pu and $\Delta P_{D,2}$= 0.08 pu MW; each perturbation influences the other neighboring subsystem, as it can be seen in Fig.2.

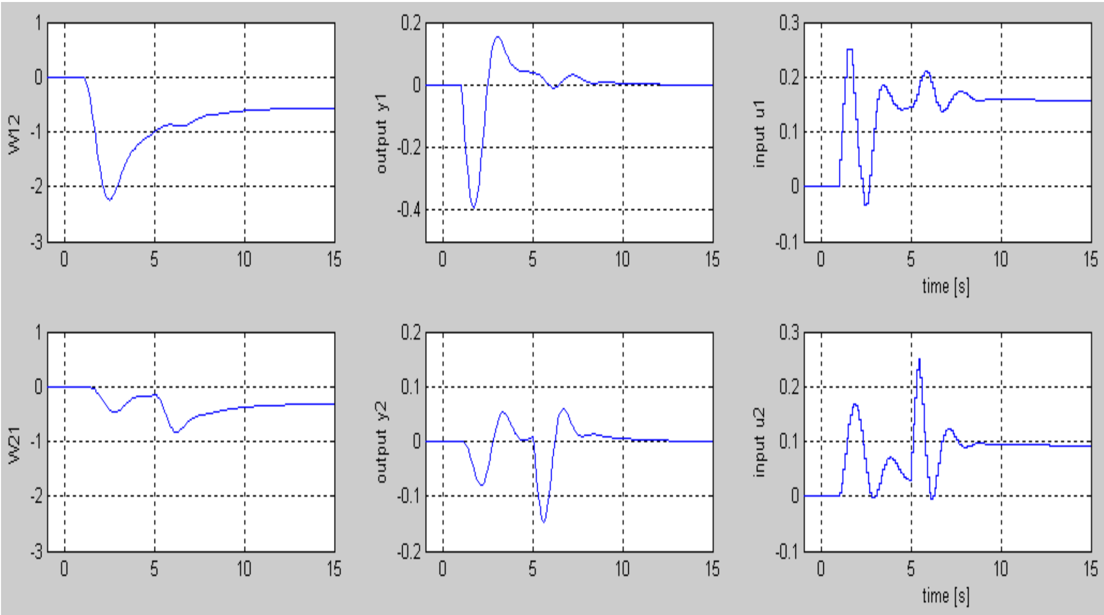

Fig. 2 – Interconnected subsystems dynamics

Figure 2 shows the evolution of the frequency deviations in each subsystem after local disturbances and also, the influence in neighboring system. With control agents the dynamics of each area become stable; for each step the inputs values are beyond imposed limits.

5. CONCLUSIONS

In this paper we have studied a multi-agent control application in power systems for the solution of Load Frequency Control. The tie-lines power flow are maintained to specified values based on communication between neighboring agents. The connections between subsystems are treated by each controller agent as a set of disturbance signals; they improve the predictions about the future evolutions of interconnections variables solving an optimization problem related to the paradigm of model-based predictive control.

Assuming that communication are reliable, the numerical example shows that it is posible to realise such distributed control method, based on autonomous agent behaviors.

REFERENCES

1. **J. M. Maciejowski**, Predictive Control with Constraints. Prentice Hall, 2002.

2. **S. J. Qin, T.A. Badgwell**, *A survey of industrial model predictive control technology*, Control Engineering Practice, Vol.11, pp.733-746, 2003.

3. K. Sycara,*Multi-agent Systems*,AI Magazine,The American Association for Artificial Intelligence, **10(2)**, pp. 79-93, 1998.

4. S. D. J. Mcarthur, E. M. Davidson, V. M. Catterson, A. L. Dimeas, N. D. Hatziargyriou, F. Ponci, T. Funabashi, *Multi-Agent Systems for Power Engineering Applications Part I: Concepts, Approaches, and Technical Challenges*, In Power Systems, IEEE Transactions on, Vol. 22, No. 4. (2007), pp. 1743-1752.

5. J. A. Rossiter, *Model-based Predictive Control - a Practical Approach*, CRC Press, 2003.

6. T. Keviczky, F. Borrelli and G. J. Balas, *Decentralized Receding Horizon Control for Large Scale Dynamically Decoupled Systems*, Automatica, December 2006, Vol. 42, No. 12, pp. 2105-2115.

7. H. Bevrani, Y. Mitani,K. Tsuji, *Robust decentralised load-frequency control using an iterative linear matrix inequalities algorithm*, IEE Proceedings - Generation, Transmission and Distribution, 2004, 151(3):pp. 347-354.

8. M.T. Alrifai, M. Zribi, *Decentralized Controllers for Power System Load Frequency Control*, ICGST International Journal on Automatic Control and System Engineering, **5(II)**, pp. 7-22, 2005.

9. M. Zribi, M. Al-Rashed, M. Alrifai, *Adaptive decentralized load frequency control of multi-area power systems*, International Journal of Electrical Power & Energy Systems, **27(8)**, pp. 575-583, 2005.

CONSIDERATIONS REGARDING ASYNCHRONOUS MOTOR ROTOR PARAMETERS DETERMINATION BY FEM

Olivian **CHIVER**, Liviu **NEAMT,** Zoltan **ERDEI,** Eleonora **POP**
North University of Baia Mare, email: olich@ubm.ro, liviu_neamt@ubm.ro, nora@ubm.ro, erdeiz@ubm.ro.

Key words: asynchronous motor, rotor parameters, finite elements method.
Abstract*:* *The paper presents some considerations about asynchronous motor rotor parameters determination, using software based on finite elements method (FEM). For this, 2D magnetostatic and time harmonic analysis will be realized, at different frequencies, in case of a three phase asynchronous motor.*

1. INTRODUCTION

The asynchronous motor rotor parameters are determined experimentally by two tests: no load test and short circuit test. Magnetization resistance and the sum between stator leakage reactance and magnetization reactance are determined on the basis of measurements realized in no load test. Based on measurements of short circuit test are determined the short circuit resistance and reactance respectively. While the rotor resistance at start moment can be determined from the short circuit resistance (the stator resistance can be measured), the rotor leakage reactance can not be separated from the stator leakage reactance. In order to determine the stator leakage reactance separately, the "removed rotor method" [4] can be used.

2. PARAMETERS DETERMINATION BY FEM

Numerical methods development, especially FEM, makes possible the simulation of any permanent or transient regime, therefore the previously presented methods can also be simulated.

The ideal no load test assumes that the rotor speed is synchronous with the rotating magnetic field generated by the stator winding (s=0), then no current is induced in rotor bars. The rotor becomes exclusively a part of the nonlinear magnetic path for the stator magnetic flux.

No load test numerical simulation by FEM can be realized by a 2D magnetostatic field analysis, the goal being the magnetization reactance determination.

In case of an asynchronous motor with squirrel cage rotor (with high bars), double layered stator winding with shortened pitch to 5/6, six notches per pole and phase, two poles pair, the required numerical model for magnetostatic analysis is presented in figure 1.

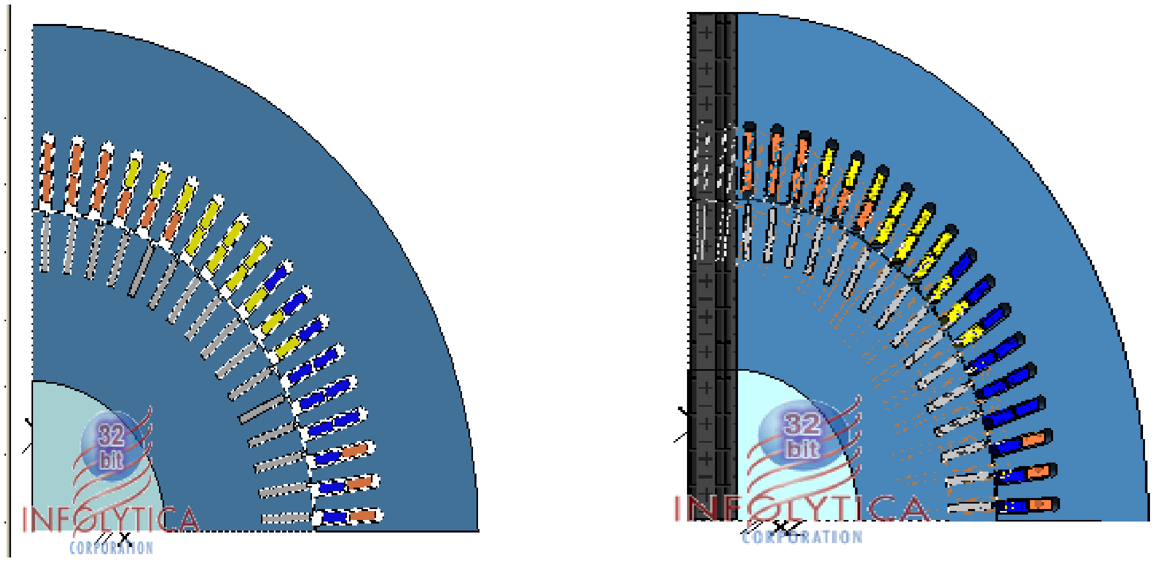

Fig. 1. The numerical model

Since the rotating electrical machines are symmetrical, the numerical model corresponds to a single pole, and the periodic boundary conditions are used.

The equivalent electrical circuit in case of no load regime is presented in *fig. 2a*. In order to realize the simulation, current sources are used.

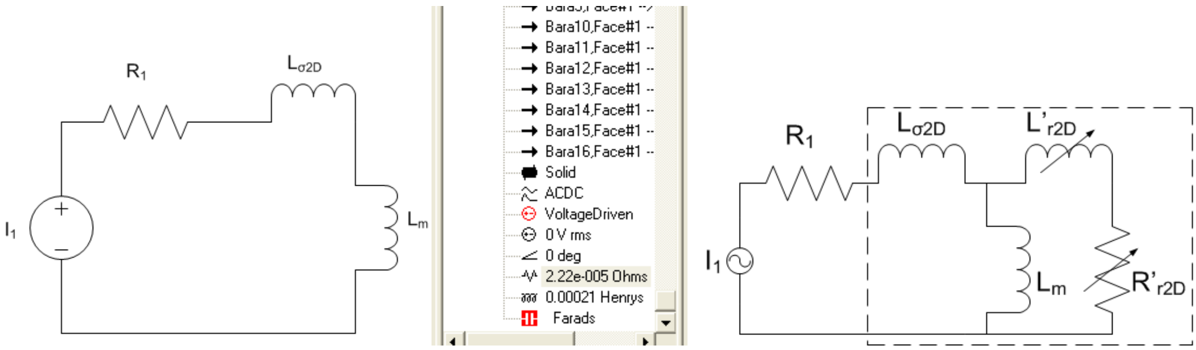

a) *b)* *c)*

Fig. 2. The equivalent electrical circuits

The stator leakage inductance $L_{\sigma 2D}$ can be determined as is described in [2].

The magnetization inductance is determined in terms of the magnetic energy W_m stored in the analyzed model (in this case a quarter of the machine) and the maximum value of the phase current I_m, respectively:

$$L_m = 4\frac{4W_m}{3I_m^2} - L_{\sigma 2D} \tag{1}$$

Rotor leakage inductance determination, both at start at nominal current and at nominal speed, requires harmonic analysis at different frequencies, the numerical model being the same with the previous one, only that the rotor bars realize together a circuit that represents the squirrel cage winding (*fig. 2b.)*.

In *fig. 2c*. the equivalent electrical circuit is presented, and both the rotor resistance and rotor reactance are in terms of the slip.

As for the magnetization inductance, it is considered constant, its value corresponding to a low voltage supply regime, the magnetic circuit being no saturated.

The circuit parameters situated inside the dashed box in *fig. 2c*. can be replaced with an equivalent resistance and inductance obtained with [1]:

$$L_{eq} = 4\frac{2W_m}{3I_{ef}^2} \qquad R_{eq} = 4\frac{P_{jr}}{3I_{eq}^2} \tag{2}$$

P_{jr} represents the Joule losses in the rotor bars, these being known trough numerical analysis, and I_{ef} represents the RMS value of the stator phase current.

Since the stator leakage inductance and the magnetization inductance are known, both the rotor leakage inductance and the rotor resistance from the active portion can be determined.

The electrical resistance and inductance of the rotor ring had not been introduced in the equivalent electrical circuit, because the values of these parameters had been considered in the numerical model as external circuit elements, this being required for a high accuracy computation of the rotor bars induced currents.

For rotor parameters determination at start moment, the harmonic numerical analysis is realized at nominal frequency, while in case of nominal speed, the frequency is $f=s_nf_n$.

The magnetic field lines are presented comparatively for two limit cases, at start moment and ideal no load regime respectively (*fig. 3.*).

In *fig. 3*. can be noticed the influence of the currents induced in rotor bars over the stator magnetic field.

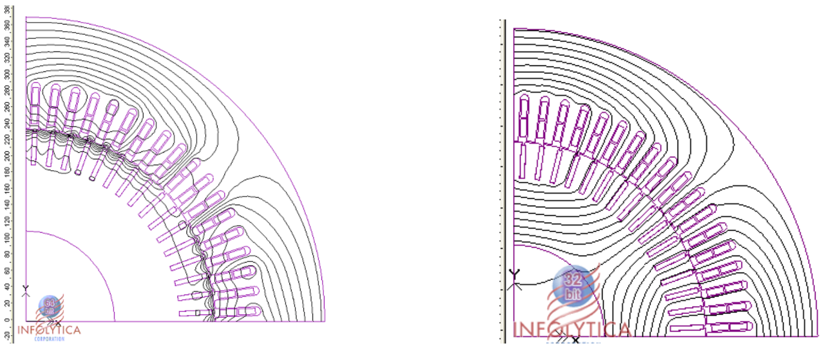

Fig. 3. Flux lines at start and at nominal speed

In case of asynchronous motors with high rotor bars or those with double squirrel cage, the rotor parameters have different values at start moment and at nominal speed, because of the non uniform current distribution in the rotor bars at high frequencies.

In *fig. 4.* the flux lines and current density in rotor bars are presented for two stator current frequencies: 50Hz (the start moment) – left, and 2.5Hz (nominal speed) – right, in case of an asynchronous motor with high bars.

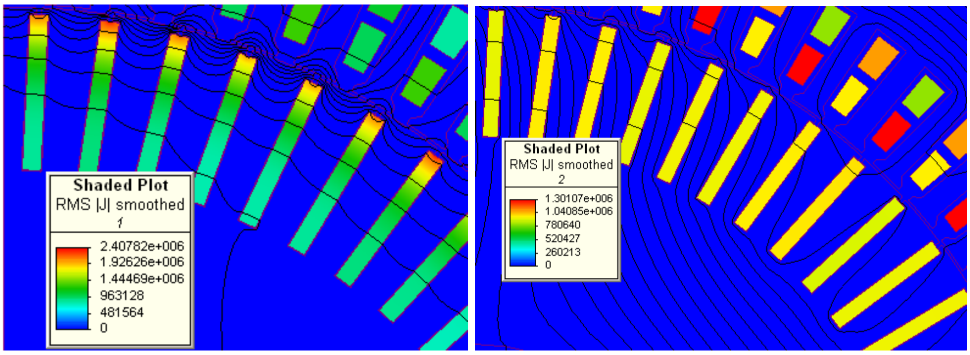

Fig. 4. The current distribution in high rotor bars at start and at nominal speed

The variation of rotor leakage inductance and the rotor resistance in terms of current frequency is presented in *fig 5.* in case of 55 kW asynchronous motor, with height of the rotor bars 25 mm, and the height/width bar ratio 8.3.

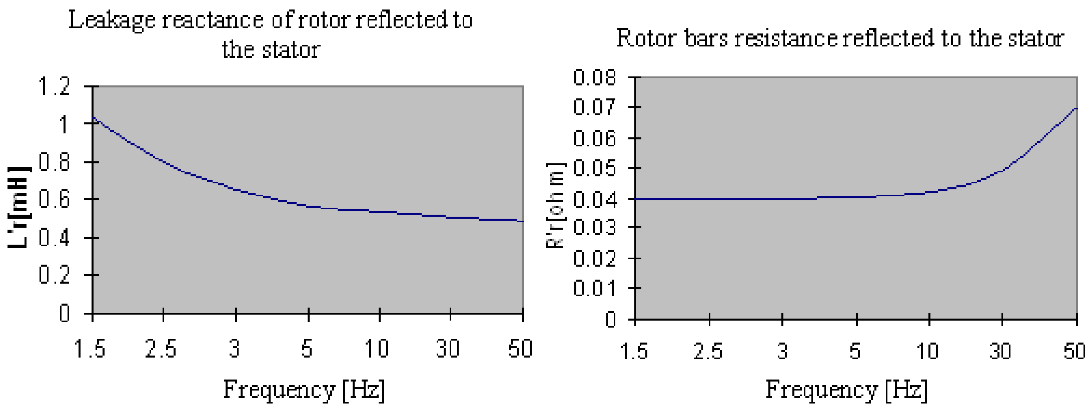

Fig. 5. The rotor leakage reactance and rotor resistance in terms of frequency

For this motor, the equivalent rotor resistance decreases from 0.07 Ω at start moment to 0.04 Ω at 3% slip, decreasing 1.75 times, while the rotor leakage inductance increases from 0.49 mH at start moment to 1.04 mH at 3% slip, increasing 2.1 times.

In order to study the rotor parameters change, have been realized models representing asynchronous motors with power in 5.5 – 1000 kW scale, and for each rotor the reduced height of the bar has been computed with relation:

$$\xi = h\sqrt{\omega_r \mu_0 \frac{b}{2b_{cr}\rho}} \tag{3}$$

Has been noted with h – high of the rotor bar, b – width of the rotor bar, b_{cr} – width of the notch, ρ – the electrical rotor bar resistivity, and $\omega_r=2\pi f_r$.

The nominal slip values have been chosen in 0.05 – 1.6 scale, in terms of the motor power, and the results regarding the value of the increasing resistance coefficient k_r in terms of the reduced height of the rotor bar ξ, for the analyzed models, are presented in *fig. 6a*.

The analytic curve that represents the variation of the increasing resistance coefficient k_r in terms of the reduced height of the rotor bar is presented comparatively.

A good concordance between analytically obtained and FEM results can be noticed.

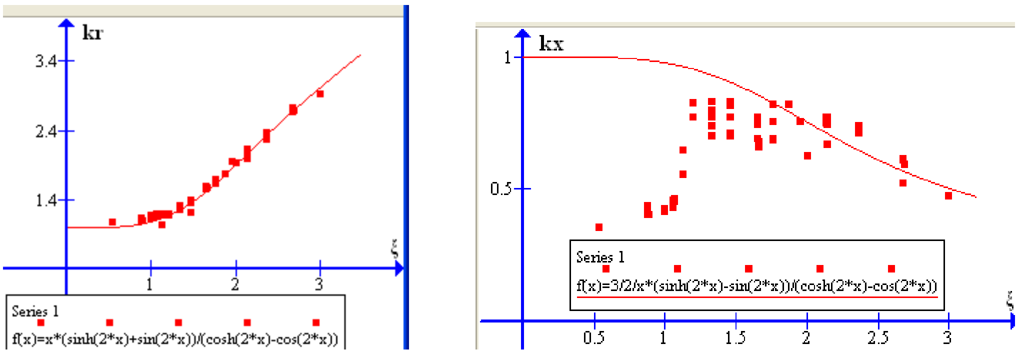

a) b)

Fig. 6. The k_r and k_x coefficient in terms of reduced height of the rotor bar, ξ

The results obtained by presented method, regarding the variation of leakage inductance from active portion of the rotor in terms of the reduced height of the rotor bar ξ, are showed in *fig 6b.*

The comparison between the decreasing coefficient values, k_x, obtained by FEM and analytically, respectively, highlights the fact that, generally, for values of the reduced height of the rotor bar ξ up to 1.66, the discrepancies are important.

The explanation consist in the following: leakage inductance of the rotor in nominal regime determined according to the presented method is higher than the leakage inductance corresponding to the start. This high value is due to the higher value of the magnetic energy stored in the model analyzed at low frequency (at nominal regime) than the magnetic energy stored in the model analyzed at nominal frequency (at start regime). Considering that this increase of the magnetic energy is only due to the leakage inductance could explain the high value of leakage inductance at nominal regime.

The detailed analysis of the models regarding the magnetic energy stored in different parts of the machine however highlights that the most important increases are in the magnetic circuit and in the air-gap.

Thus, if at start moment the magnetic energy stored in the magnetic circuit is insignificant in comparison with the total energy, at nominal regime, this energy increases 20-30 times, up to 10%. At start moment, the magnetic energy stored in the air-gap represents about 30% from the total magnetic energy, and at nominal speed this energy comes up to 50%.

Based on these observations, for rotor slots leakage inductance determination, only the magnetic energy stored in the rotor slots has been taken into consideration, the relation of dependence being presented in (2).

In order to established the k_x coefficient, it has been taken into consideration that only leakage inductance corresponding to the rotor bar portion is affected by nonuniform distribution of the current.

In figure 7., k_x coefficient values obtained by FEM, based on magnetic energy stored in rotor slots, are presented in terms of the reduced height of the rotor bar ξ.

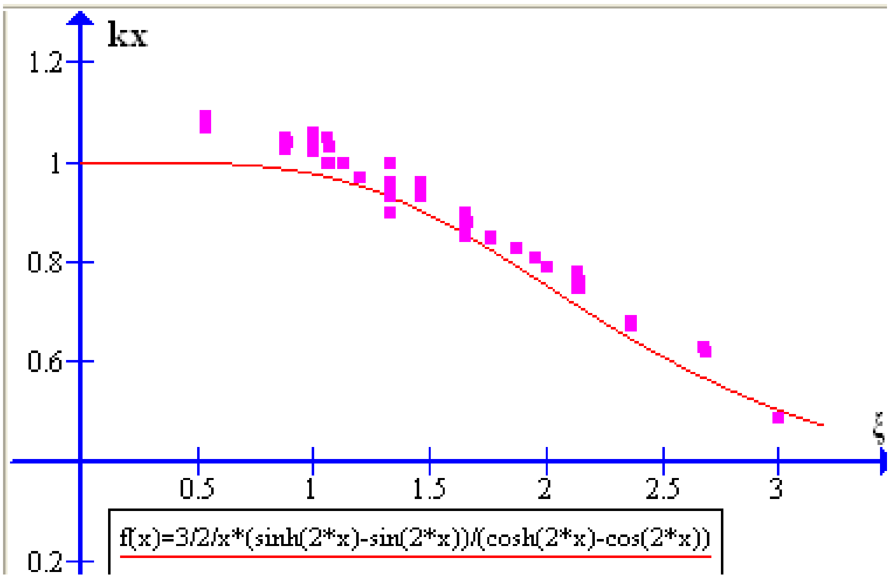

Fig.7. The k_x coefficient in terms of reduced height of the rotor bar, ξ, obtained by magnetic energy stored in rotor slots

This time, a good concordance between analytically and FEM obtained results can be noticed.

The values higher than one (up to 1.06), are due to the fact that in case of squirrel cage rotor without high bars, at start moment the current distribution is uniform like at nominal speed, *fig. 8*.

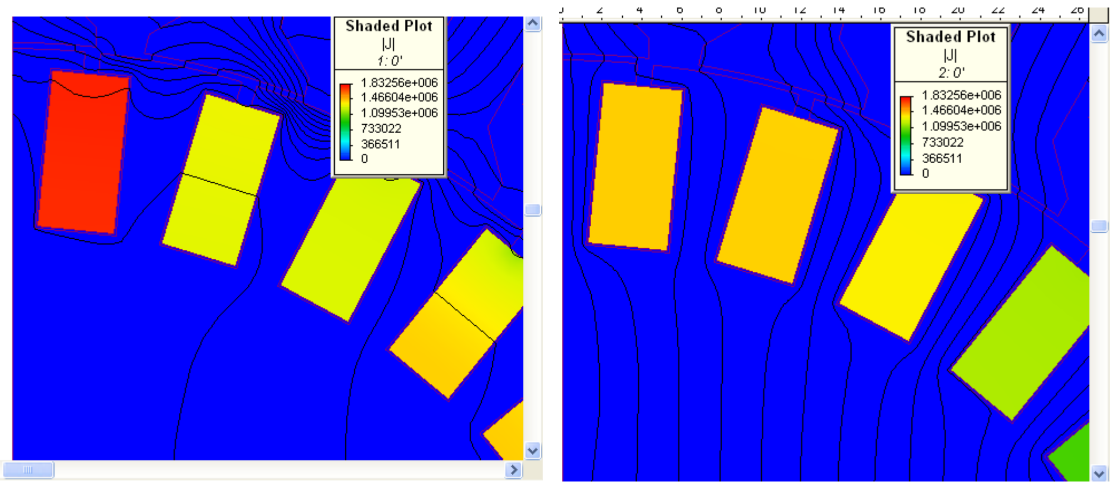

50 Hz 2.5 Hz

Fig. 8. The rotor bars current distribution in case of rotor without high bars

On the other hand, if at start moment the current distribution is uniform, more field lines close by rotor slots (*fig. 8.*), and thus the value of the magnetic energy stored in rotor slots is higher than that at nominal speed, although not all these lines represent the leakage field.

3. CONCLUZIONS

The computation of the rotor slots leakage inductance based on the first presented method, leads to satisfactory results only in case of the machines with the reduced height of the rotor bar generally higher than 1.66, in this case the rotor bars current distribution being nonuniform.

The computation of the rotor leakage inductance and of k_x coefficient based on the magnetic energy stored in the rotor slots highlights a good concordance between analytically and FEM results.

Thus can be noticed that the rotor leakage inductance determination from magnetic energy stored in rotor slots has a satisfactory accuracy, the method could be applied in general case, regardless of rotor bars shape.

REFERENCES

1. Bianchi N., „*Electrical machine analysis using finite elements”*, CRC Taylor & Francis Group, 2005;

2. Chiver O., Micu E., Barz C., „*Stator winding leakage inductances determination using Finite Elements Method"*, 11th International Conference on Optimization of Electrical and Electronic Equipment OPTIM'08, Braşov, România, May 22-24, 2008;

3 Cioc I., Nica C., „Proiectarea maşinilor electrice", Ed.D.P., Bucuresti 1994;

4. Draganescu O. Gh., „*Incercarile maşinilor electrice rotative*", Ed. Tehnică, Bucureşti 1987;

5. Fireţeanu V., "Modele numerice în studiul şi concepţia dispozitivelor electrotehnice", Ed. Matrix Rom, Bucureşti, 2004;

6. MagNet User's Guide;

7. www.infolytica.com/.../doccenter.

SWITCHED RELUCTANCE MOTOR OPTIMAL GEOMETRY DESIGN

Liviu **NEAMŢ**, Arthur **DEZSI**

North University of Baia Mare, Romania, Eaton Electrical Group, Romania

liviu_neamt@ubm.ro

Key words: SRM, Finite Element Method, Design

Abstract*: This paper deals with the Switched Reluctance Motor (SRM) analysis using Finite Element Method (FEM) for geometrical optimization in terms of volume ratio of torque on the rotor, the so-called specific torque. The optimization parameter is the pair: stator and rotor pole angles, which forms a crucial part of the design process.*

1. INTRODUCTION

In the world market for electrical drives applications some domains, such as electric traction motor, pumps and compressors at high speeds, robots and numerically controlled machine tools, aeronautics and space technical, computer peripherals, etc., became clearly dominated by the stepper motor - electronic converter assembly, known as SRM.

These led, unsurprisingly, to a huge interest from researchers, in obtaining a more efficient motor and electronic converter and in development of design methods less influenced by simplified assumptions with a high generality.

2. SRM PRELIMINARY DESIGN

SRM design should be initiated with a first step, so-called pre sizing, which provides an initial set of geometric data.

Obtaining the diameter and length of stepper motor is considered in several works [1], [2], [3] stems from the recommendations, in accordance with ISO, of the International Electrotechnical Commission (IEC), by assimilation with asynchronous machine. The preliminary selection of frame size goes automatically at the outer diameter of the stator. The outer diameter of the stator is fixed in millimeters:

$$D_e = (framesize - 3) \cdot 2 , \tag{1}$$

The rotor diameter is initially considered as the frame size, the feed-backs from design procedure leading to required changes.

Once established these key dimensions it'll proceed to calculate the stator, β_S and the rotor, β_R, pole arcs both expressed in radians, which is recommended to satisfy the following relationships [2], [3], providing a maximum torque without engine to remain locked or to lose steps:

$$\beta_S \le \beta_R , \tag{2}$$

$$\beta_S > \theta_p , \tag{3}$$

$$\beta_S + \beta_R < \frac{2\pi}{Z_R} , \tag{4}$$

The three relations describe a triangle so the SRM will function optimally only if the stator and rotor pole angles will be found in this triangle. Fig.1. shows feasible triangle for a 8/6 machine. The region below OE represents condition 1, the region above GH represents condition 2 and the region below DF represents condition 3. For example, if $\beta_S = 20^0$ then $20^0 < \beta_R < 40^0$.

Identification of optimal values for arcs involves calculating the maximum torque for different combinations, as long as relations (2) - (4) only set some restrictions. Since determining the maximum torque is subject to there overall package size of the resulting motor, this step is one that sends to the initial phase of design for each new tested value of the arc.

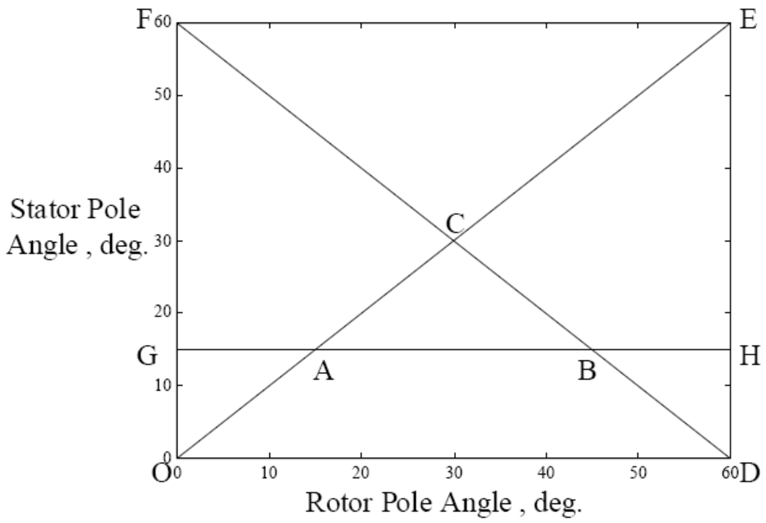

Fig. 1 - Feasible triangle for a 8/6 machine

Determination of machine torque can be done analytically from a number of simplifying assumptions and magnetic equivalent circuit models.

FEM remains the best analysis tool. The easy way to accomplish the non linearity and the complicated structure of the materials, great accuracy of the simulation, reduced costs, speed of analysis permit to take into account a lot of models and choose the best fitting of a desired imputed condition.

Will be considered a SRM prototype 8/6 which has the following characteristics:

Power output: $P_{kw} = 3728$ [W]

Speed: $N = 1500$ $[rot/\min]$

Peak current: $i_p = 13$ [A]

Input AC voltage $V_{ac} = 480$ [V]

The torque to be developed by the machine is:

$$T = \frac{P_{kw}}{2\pi\left(\frac{N}{60}\right)} = \frac{3728}{2\pi\left(\frac{1500}{60}\right)} = 23.7459\ [N \cdot m], \tag{5}$$

The machine will be designed with an IEC frame size of 100. The outer diameter of the stator is fixed as follows:

$$D_0 = (gabarit - 3) \cdot 2 = (100 - 3) \cdot 2 = 194\ [\text{mm}] \tag{6}$$

The maximum stack length for frame 100 is restricted to 200 mm: $L = 200$ [mm]

For a machine of this frame size, a practical air-gap length can be assumed to be: $\delta = 0.5$ [mm]

The bore diameter D equal to the frame size is selected: D=100 [mm].

The remaining sizes are determined based on relatively simple relations and are not elements of variability within the meaning of optimization in this paper.

So the only undetermined sizes are stator and rotor pole arcs. Using Fig.1, and considering only the integer values of the angles resulted from triangle ABC, a total of 496 possible combinations become valid. Removing the combinations when $\beta_s = \beta_r$ and all combinations over $\beta_r - \beta_s > 5°$, because it follows a very high torque oscillation it remain to be analyzed 80 possible combinations of rotor polar arc and polar arc stator, Fig. 2.

Arcul polar rotoric [°]

Arcul polar statoric [°]

	15	16	17	18	19	20	21	22	23	24	25	26	27	28	29	30	31	32	33	34	35	36	37	38	39	40	41	42	43	44	45
15	0	1	2	3	4	5	6	7	8	9	10	11	12	13	14	15	16	17	18	19	20	21	22	23	24	25	26	27	28	29	30
16	-1	0	1	2	3	4	5	6	7	8	9	10	11	12	13	14	15	16	17	18	19	20	21	22	23	24	25	26	27	28	29
17	-2	-1	0	1	2	3	4	5	6	7	8	9	10	11	12	13	14	15	16	17	18	19	20	21	22	23	24	25	26	27	28
18	-3	-2	-1	0	1	2	3	4	5	6	7	8	9	10	11	12	13	14	15	16	17	18	19	20	21	22	23	24	25	26	27
19	-4	-3	-2	-1	0	1	2	3	4	5	6	7	8	9	10	11	12	13	14	15	16	17	18	19	20	21	22	23	24	25	26
20	-5	-4	-3	-2	-1	0	1	2	3	4	5	6	7	8	9	10	11	12	13	14	15	16	17	18	19	20	21	22	23	24	25
21	-6	-5	-4	-3	-2	-1	0	1	2	3	4	5	6	7	8	9	10	11	12	13	14	15	16	17	18	19	20	21	22	23	24
22	-7	-6	-5	-4	-3	-2	-1	0	1	2	3	4	5	6	7	8	9	10	11	12	13	14	15	16	17	18	19	20	21	22	23
23	-8	-7	-6	-5	-4	-3	-2	-1	0	1	2	3	4	5	6	7	8	9	10	11	12	13	14	15	16	17	18	19	20	21	22
24	-9	-8	-7	-6	-5	-4	-3	-2	-1	0	1	2	3	4	5	6	7	8	9	10	11	12	13	14	15	16	17	18	19	20	21
25	-10	-9	-8	-7	-6	-5	-4	-3	-2	-1	0	1	2	3	4	5	6	7	8	9	10	11	12	13	14	15	16	17	18	19	20
26	-11	-10	-9	-8	-7	-6	-5	-4	-3	-2	-1	0	1	2	3	4	5	6	7	8	9	10	11	12	13	14	15	16	17	18	19
27	-12	-11	-10	-9	-8	-7	-6	-5	-4	-3	-2	-1	0	1	2	3	4	5	6	7	8	9	10	11	12	13	14	15	16	17	18
28	-13	-12	-11	-10	-9	-8	-7	-6	-5	-4	-3	-2	-1	0	1	2	3	4	5	6	7	8	9	10	11	12	13	14	15	16	17
29	-14	-13	-12	-11	-10	-9	-8	-7	-6	-5	-4	-3	-2	-1	0	1	2	3	4	5	6	7	8	9	10	11	12	13	14	15	16
30	-15	-14	-13	-12	-11	-10	-9	-8	-7	-6	-5	-4	-3	-2	-1	0	1	2	3	4	5	6	7	8	9	10	11	12	13	14	15

Fig. 2 - Combinations analyzed

3. SRM OPTIMIZATION

All 80 combinations of stator and rotor arc are carried out by FEM analysis using Infolytica Magnet V 7 [5].

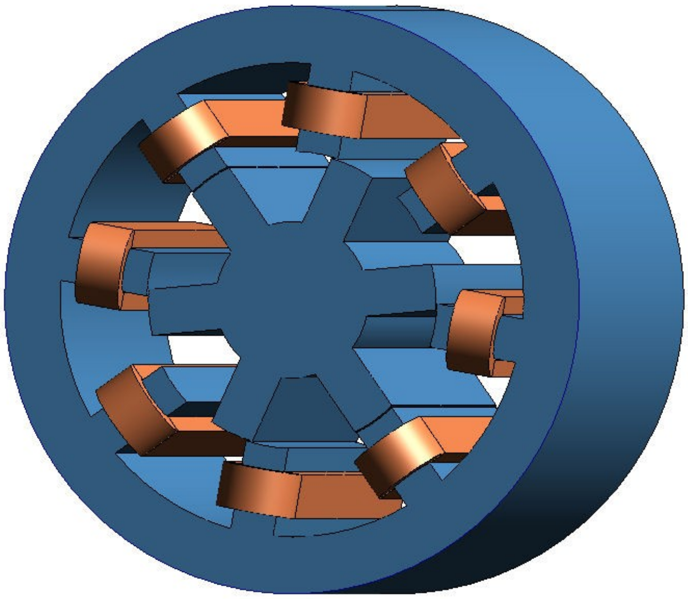

Fig. 3 – Optimized SRM

For example the geometry, final mesh and the magnetic field spectrum are presented for two combinations:

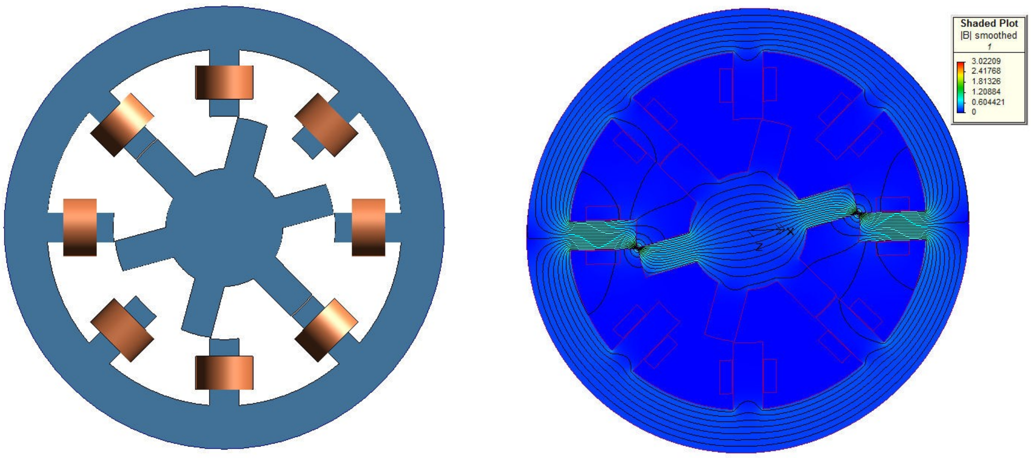

Fig. 4 – SRM with $\beta_s = 15^0$, $\beta_r=16^0$. Resulted maximum torque of 22.37719369403 [Nm].

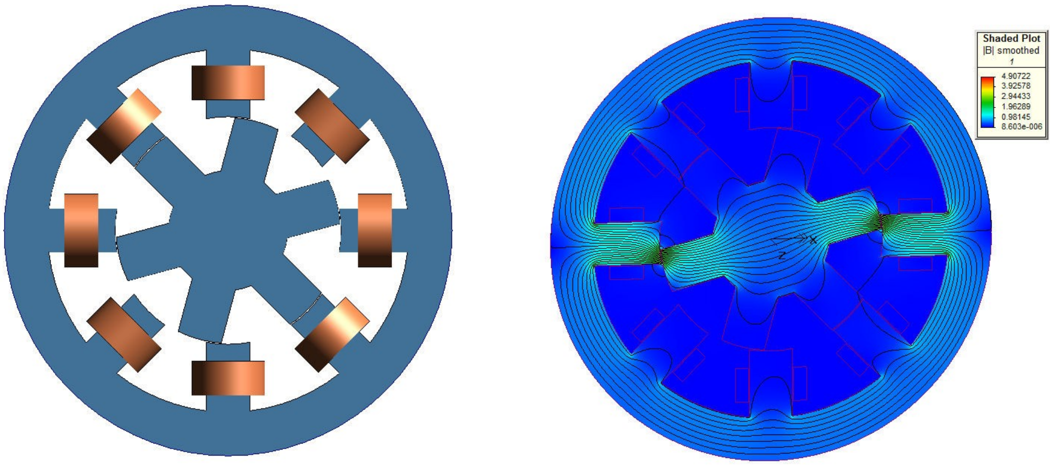

Fig. 5 – SRM with $\beta_s = 22^0$, $\beta_r=23^0$. Resulted maximum torque of 22.96590710053 [Nm].

Below are presented, in graphical form, the values of maximum torque for the 80 analyzed combinations of arcs stator – rotor:

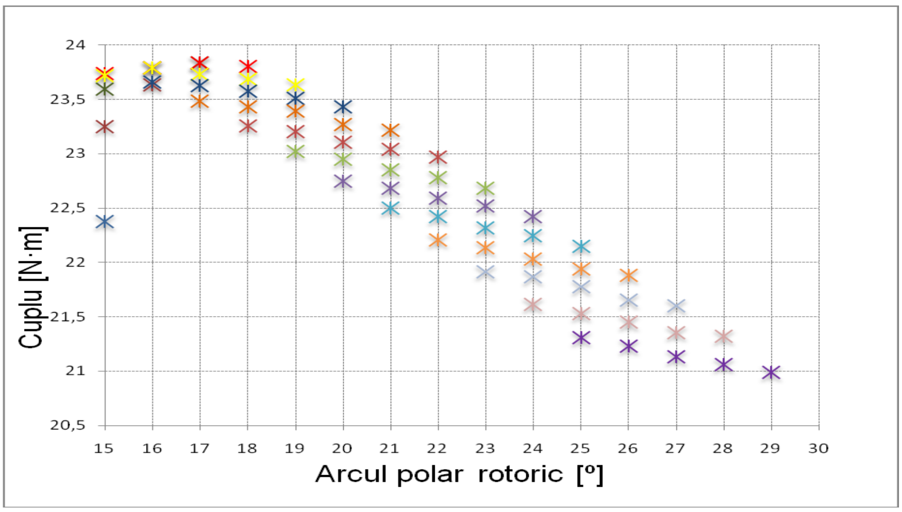

Fig.6. Maximum SRM torque

Choosing the optimal configuration implies to find the maximum of torque function, summarized below:

Table 1.

β_S[°]	β_R[°]				
	17	18	19	20	21
16	23.63229790367	23.79089221673	23.786169113	23.78645798388	23.65620882183
17	x	23.83713248871	23.837004845	23.729893902	23.62874549198
18	x	x	23.80226305215	23.68337550118	23.57710280044

Considering that the optimization process is done in terms of maximum torque, the optimum model produces a 23.83713248871 [Nm] torque for the stator pole arc, $\beta_S = 17^0$ and the rotor pole arc, $\beta_R = 18^0$.

Optimized model must be examined in detail to validate the results.

For these the maximum torque values, fig.5, respectively linkage magnetic flux values, fig. 6, for different rotor positions must be determined.

Using the same FEM software, Magnet, V. 7, these computations are realized in the post processing stage of analysis.

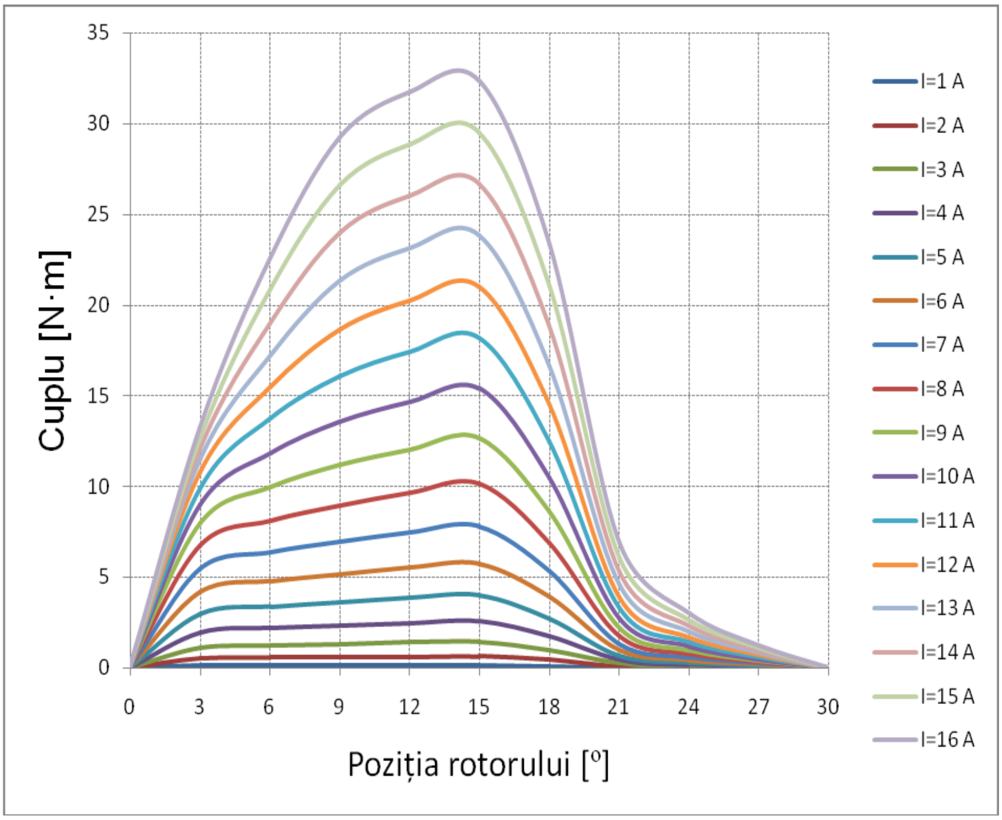

Fig.7. Maximum torque depending on rotor position

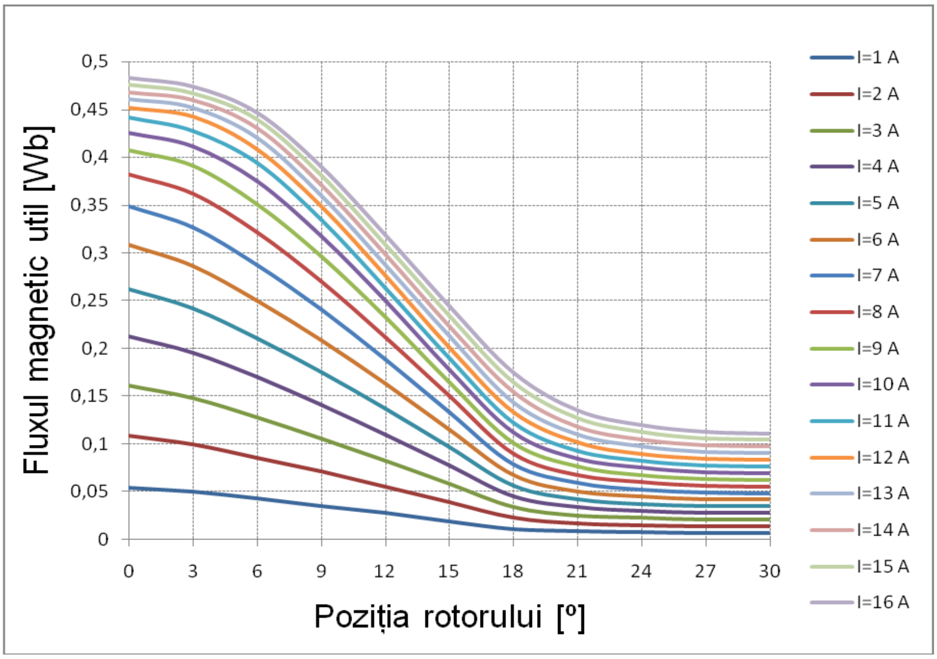

Fig.8. Linkage magnetic flux depending on rotor position

4. CONCLUSIONS

It was presented a FEM based design methodology to obtain an optimum combination of stator and rotor pole angles for a 8/6 SRM in terms of maximum torque for one phase fed at a time.

This start with classical pre sizing of the machine for establishing basic geometry of a basic SRM model. Based on “feasible triangle” and other restrictions the basic SRM will generate a number of available configurations.

FEM analysis of these models and maximum torque computation will identifies the optimum model of the SRM.

Of course a complete analysis of the resulted optimum SRM must be done to certify the choice.

REFERENCES

1. Praveen V, *Design of Switched Reluctance Motor and Development of a Universal Controller for Switched Reluctance and Permanent Magnet Brushless DC Motor Driver,* Ph.D. Dissertation, Blacksburg-Virginia, 2001.

2. Krishanan R, *Switched Reluctance Motor Drives: Modeling,. Simulation, Analysis, Design, and Applications*,CRC Press, 2001.

3. Miller, TJE, S*witched Reluctance Motors and their Control*, Magna Physics Publishing and Clarendon Press, Oxford, 1993.

4. Torkaman, H. Afjei E, *Comprehensive study of 2-D and 3-D finite element analysis of a switched reluctance motor***.** J. Applied Sci**.,** 8: 2758-2763, 2008.

5. Magnet CAD Package, *User Manual*. Infolytica Corporation Ltd., Montreal, Canada, 2007**.**

6. Faiz J, Ganji B, De Doncker R. W, Fiedler J.O, *Electromagnetic Modeling of Switched ReluctanceMotor Using Finite Element Method***,** IEEE Industrial Electronics, IECON 2006.

7. Lee J. W, Kim H. K, Kwon B. I, Kim B. T, *New Rotor Shape Design for Minimum Torque Ripple of SRM Using FEM,* IEEE Transactions on Magnetics, Vol. 40, No. 2, March 2004.

COMPARISON BETWEEN ANALOG AND DIGITAL FILTERS

Zoltan **ERDEI**[*], Paul **BORLAN**[**] and Olivian **CHIVER**[*]

[*] *North University of Baia Mare, Romania*
erdeiz@yahoo.com

Key words: analog filters, digital filters, signal proccesing

Abstract: *Digital signal processing(DSP) is one of the most powerful technologies and will model science and engineering in the 21st century. Revolutionary changes have already been made in different areas of research such as communications, medical imaging, radar and sonar technology, high fidelity audio signal reproducing etc. Each of these fields developed a different signal processing technology with its own algorithms, mathematics and technology, Digital filters are used in two general directions: to separate mixed signals and to restore signals that were compromised in different modes. The objective of this paper is to compare some basic digital filters versus analog filters such as low-pass, high-pass, band-pass filters. Scientists and engineers comprehend that, in comparison with analog filters, digital filters can process the same signal in real-time with broader flexibility. This understanding is considered important to instill incentive for engineers to become interested in the field of DSP. The analysis of the results will be made using dedicated libraries in MATLAB and Simulink software, such as the Signal Processing Toolbox.*

1. INTRODUCTION

Analog filters are a first layer block in signal processing, often used in electronics. Passive filters have been the base of communications since the 1920's and are of considerable importance for frequencies situated between 100 and 500 kHz. Hundreds, if not thousands of types of passive filters have been developed in order to satisfy the needs of different applications. However most filters can be described by few common charactheristics. First of them is the frequency domain of their bandpass. The bandpass of a filter is frequency domain over which an input signal will pass. Signals of frequencies that are not in the bandpass will be attenuated.

2. LOWPASS FILTER

Lowpass filters allow low frequency signals to pass, while they block high frequency signals. The concept of lowpass filter exists in various forms, including electronic circuits, digital algorithms used to process data sets, acoustic barriers, image processing etc. Low-pass filters play the same role in signal processing that moving averages do in some other fields, such as finance; both tools provide a smoother form of a signal which removes the short-term oscillations, leaving only the long-term trend. In equation (1) you can see the break frequency, also called the turnover frequency or cutoff frequency (in Hz).

$$f_c = \frac{1}{2\pi\tau} = \frac{}{2\pi} \tag{1}$$

where R is the resistor, with a value in ohms, and C is the capacitor, with a value in Farads.

In figure 1 you can see the analog realization of a lowpass filter and in figure 2 you can see the output waveform of a lowpass filter.

Same filter response can be obtained using a digital filter as shown by the system block diagram in figure 3. The analog signal x(t) is converted into a discrete-time signal x(n), which is processed by the digital filter, to yield a discrete-time output y(n). Finally, the discrete output y(n) is converted into an analog form y(t). The cutoff frequency of digital filter response $H(e^{j\acute{\omega}})$ is related to the analog cutoff frequency through the important analog-digital frequency relation

$$\acute{\omega} = \acute{\Omega} T \tag{2}$$

where T(s) is the sampling interval of discrete-time system.

Hence, the unit of analog frequency, Ώ, is radians/s and while the unit of digital frequency, ώ, is radians.

The digital filter can be realized using a Digital Signal Processor (DSP). The DSP can be programmed to act as any kind of filter. This is one of the main advantages of digital systems.

In digital processing the signal is represented by a signal of numbers that are stored and then processed.

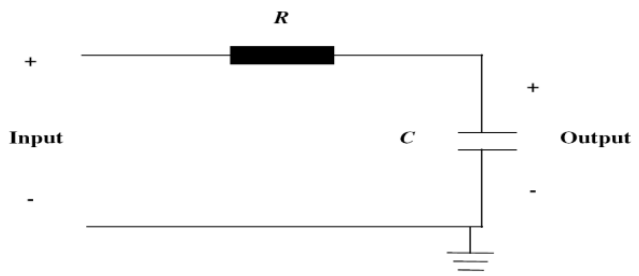

Figure 1. Analog realization of lowpass filter

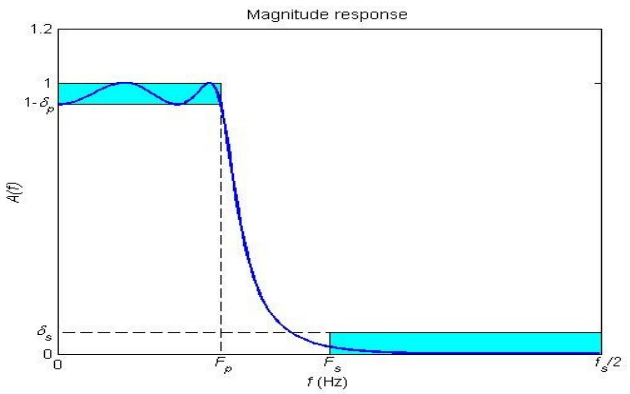

Figure 2. Output waveform of a lowpass filter

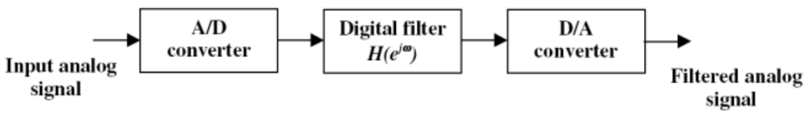

Figure 3. System block diagram of a digital lowpass filter

3. EXAMPLE

Using Mathlab the model is built in the Simulink and implemented on the ECG signal. In the model the Designed Low pass, high pass and notch filter has been cascaded figure shows the basic model used.

ECG amplifier gives the unfiltered output which contains the noise artifacts. The Power spectrum in the Figure Shows In the unfiltered signal the power line interferences as well as the high frequency noise is present. This nose is to be eliminated so that no information in the ECG signal missing. Figure 4 shows the Basic block diagram for the system used for the filtration of the ECG signal.

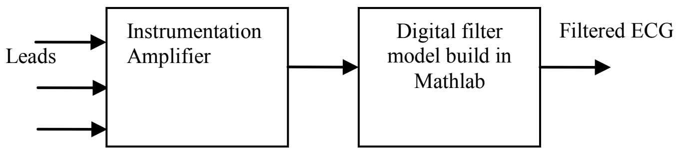

Figure 4 Block Diagram for system used for the noise reduction in the ECG

Below are presented the different lead combinations clearly showing the Noise reduction due to different filters. The filters work satisfactorily.

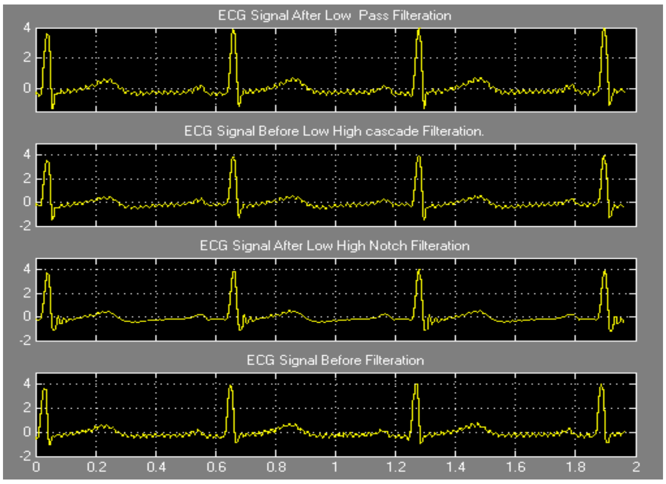

Figure 5.a ECG lead I signal of Chebyshev- II cascade filter.

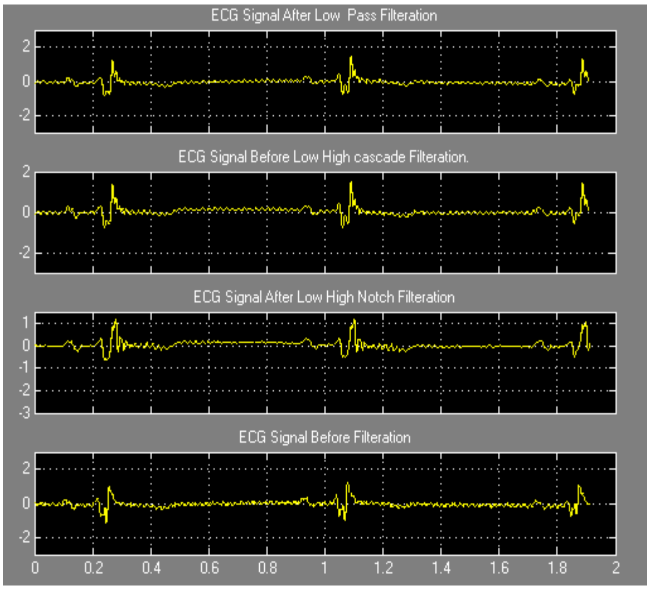

Figure 5.b ECG lead III signal of Chebyshev-II cascade filter.

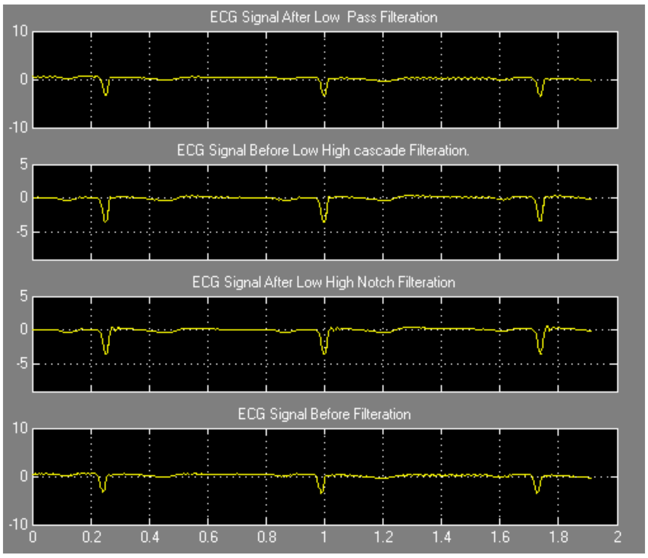

Figure 5.c ECG lead aVR signal of Chebyshev-II cascade filter.

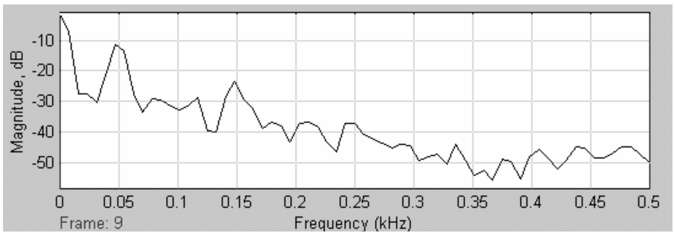

Figure 6.a Frequency Spectrum for Chebyshev II Filter Before Filtration of the ECG Signal

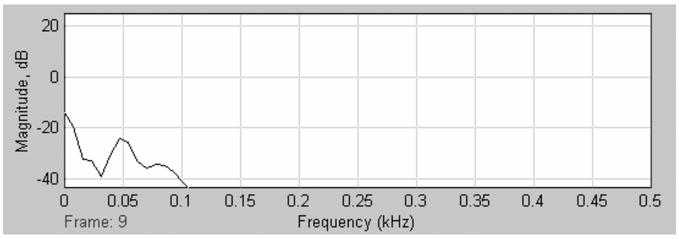

Figure 6.b Frequency Spectrum for Chebyshev II Filter after Filtration of the ECG Signal.

4. CONCLUSIONS

With visualization of above results by appropriate design if the Digital Chebyshev type II Filter the noise in the ECG signal can be effectively reduced.

Throughout our experiments we used MATLAB and SIMULINK in order to simulate de filter and process the input signal.

Some of the key features that distinguish digital filters from analog filters are: digital filters are programmable, implemented using software packages, can easily be changed or updated without affecting their circuitry (hardware), can be designed, tested and implemented on a general purpose computer, are independable of physical variables such as temperature, tolerances of elements, noise, fluctuations or inteferences. Analog filters use elements that are environment dependent, and any filter change is usually hard to implement and a complete design is often required.

REFERENCES

1. Wai-Kai Chen, "*Passive, active and digital filters*", Ed. CRC Press, 2006

2. Robert J. Shilling, Sandra L. Harris, "*Fundamentals of digital signal processing using Matlab*", Ed. Thomson, 2005

3. Steven W. Smith, "*The scientist and engineer's guide to digital signal processing*", 2nd edition, California Technical Publishing, 1999

4. MAHESH S. CHAVAN *Application of the Chebyshev Type II Digital Filter For Noise Reduction* In ECG Signal Proceedings of the 5th WSEAS Int. Conf. on Signal Processing, Computational Geometry & Artificial Vision, Malta, September 15-17, 2005 (pp1-8)

5. Scokolow M., Mcllory M.B. and Cheithen,M.D *' ClinicalCardiology*'; 5th ed (VALANGEMedical Book, 1990).

6. P.K.Kulkarni,Vinod Kumar,“ *Removal of power line interference and baseline wonder using real time Digital filter*”, Proceedings of international conference on computer application in electrical engineering Recent advantages. Roorkee, India. September 1997, pp 20-25.

7. Huta, J.C. and Webster. J.G. 1973, “*60 Hz Interferences Electrocardiography*”, *IEEE trans. BME* -20, pp 91-101.

8. Marques.De.Sa.J.P. “*Digital FIR filtering for removel of baseline wonder*,” *Journal of Clinical Engineering* vol. pp. 235-240.

9. Yi-Sheng, Zhu,et al. “ *P-wave detectionby an adaptive QRS-T cancellation technique*”.1987

AN ECONOMICAL AND TECHNICAL CASE STUDY FOR A SMALL HYDROPOWER SYSTEM

Dumitru Dan **POP**[1], Vasile Simion **CRĂCIUN**, Liviu **Neamţ,** Radu **Tîrnovan**, Teodor **VAIDA**

Technical University of Cluj Napoca, dan.pop@eps.utcluj.ro
Technical University of Cluj Napoca, vasile.craciun@edr.utcluj.ro
North University of Baia Mare liviu_neamt@ubm.ro
Technical University of Cluj Napoca, radu.tirnovan@eps.utcluj.ro
Technical University of Cluj Napoca, teodor.vaida@eps.utcluj.ro

Key words: hydropower system, RETScreen, renewable energy, turbine

Abstract*:* *This paper presents a case study regarding the economical and technical parameters of a hydropower system for a mountain chalet - hotel. The calculations are made using RETScreen software starting from the average flow values of the considered river, and according to this, the hydro power plant equipments are chosen. In this case study the hydropower system is connected to central grid but also having its own storage backup system, part of the energy is consumed by the mountain chalet – hotel and the remaining energy is delivered to the central grid.*

1. INTRODUCTION

The environment pollution and energy crisis are the two most concerned problems around the world. In order to solve these problems, renewable energy was developed to replace part of the energy supply as an alternative for replacing classical fuels. Therefore, renewable energy is the second contributor to the world electricity production. Most of the electricity generated from renewables comes from hydropower plants followed by other renewables including: biomass, solid waste, geothermal, solar, wind, tide, and others. [5] Hydroelectricity is one of the most mature forms of renewable energy, providing more than 19% of the world's electricity consumption from both large and small power plants. Small-scale hydropower is one of the most cost-effective and reliable energy technologies to be considered for providing clean electricity generation. It is also environmentally benign. Small

[1] ACKNOWLEDGMENT: This paper was supported by the project "Improvement of the doctoral studies quality in engineering science for development of the knowledge based society-QDOC" contract no. POSDRU/107/1.5/S/78534, project co-funded by the European Social Fund through the Sectorial Operational Program Human Resources 2007-2013.

hydro is in most cases “run-of-river”; in other words any dam or barrage is quite small, usually just a weir, and little or no water is stored. Therefore run-of-river installations do not have the same kinds of adverse effect on the local environment as large-scale hydro (they do not have negative effects to the environment such as replacement of settlements, loss of historical sites and agricultural fields, destruction of ecological life). [12]

Each hydro site is unique, since about 75% of the development cost is determined by the location and site conditions. Only about 25% of the cost is relatively fixed, being the cost of manufacturing the electromechanical equipment. The development of small hydro projects typically takes from 2 to 5 years to complete, from conception to final commissioning. This time is required to undertake studies and design work, to receive the necessary approvals and to construct the project. Once constructed, small hydro plants require little maintenance over their useful life, which can be well over 50 years. Normally, one part-time operator can easily handle operation and routine maintenance of a small hydro plant, with periodic maintenance of the larger components of a plant usually requiring help from outside contractors. [1]

Although there is no universally agreed definition for ‘‘small hydro’’, the upper limit varies between 2.5 and 25MVA and a maximum of 10MW is the most widely accepted value worldwide. The terms mini- and micro-hydro are also used to refer to groupings of capacity below the ‘‘small’’ designation. Generally in industrial terms, mini- and micro-hydro typically refer to schemes below 2MW and below 500kW, respectively. These are arbitrary divisions and many of the principles involved apply to both smaller and larger schemes. [4]

Small hydropower systems allow achieving self-sufficiency by using the best as possible the scarce natural resource that is the water, as a decentralized and low-cost of energy production, since they are in the forefront of many developing countries. In Europe the development of small hydroelectricity grows up since the seventy decade, essentially, caused by the world energy crisis, and the concerns of negative environmental impacts associated to the energy production. Hydropower is the most important energy source in what concerns no carbon dioxide, sulphur dioxide, nitrous oxides or any other type of air emissions and no solid or liquid wastes production. The introduction of innovative solutions coupled to renewable energy technologies should contribute to a substantial global reduction in emission of CO2 and other gases, which are responsible for greenhouse effects. The hydroelectric power plant utilizes a natural or artificial fall of a river and enhances the main advantages comparing with other electricity sources, namely saving consumption of fossil, fuel, or firewood, being self-sufficient without the need of imported components. [11]

Hydroelectricity is now recognized as key technologies in bringing renewable electricity to rural populations in developing countries, many of whom do not have access to electric power. [7] Typically, small hydro generation is located close to the end-user which reduces or eliminates transmission losses and it gives independence from the world’s fossil fuel fluctuations. [6]

2. DESCRIPTION OF SMALL HYDROPOWER SYSTEM

A hydropower system has the following mechanical and electrical components: a water turbine that converts the energy of flowing or falling water into mechanical energy that drives a generator which generates electrical power, a control mechanism to provide stable electrical power and electrical transmission lines to deliver the power to its destination. [2]

Hydropower systems use the energy in flowing water to produce electricity or mechanical energy. Although there are several ways to harness the moving water to produce energy, run-of-the-river systems, which do not require large storage reservoirs, are often used for microhydro, and sometimes for small-scale hydro, projects. For run-of-the-river hydro projects, a portion of a river's water is diverted to a channel, pipeline, or pressurized pipeline (penstock) that delivers it to a waterwheel or turbine. The moving water rotates the wheel or turbine, which spins a shaft. The motion of the shaft can be used for mechanical processes, such as pumping water, or it can be used to power an alternator or generator to generate electricity. This fact sheet will focus on how to develop a run-of-the-river project. [8] In fig. 1 is presented a functional scheme of a small hydropower

The amount of power available from a hydropower system is directly related to the flow rate, head, the force of gravity and a efficiency factor. The theoretical power output (in kW) can be calculated using the following equation:

$$P = Q \cdot H \cdot g \cdot e \tag{1}$$

where:

Q = usable flow rate (m^3/s);

H = Gross head (m);

g = Gravitational constant (9.8 m/s^2);

e = efficiency factor (0.5 to 0.7).

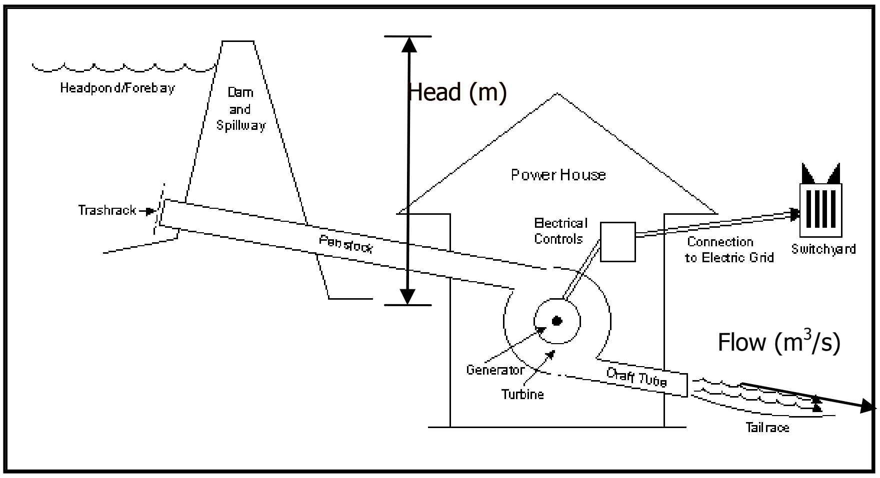

Fig. 1 - Small Hydro System Description

There are two types of turbines, impulse and reaction. For each application the turbine is chosen depending on the head and flow available. In table 1 we present different types of water turbines. [2]

Table1. Transposing principle

Turbine runner	High head (more than 100 m)	Medium high (20 to 100 m)	Low head (5 to 10 m)	Ultra-low head (less than 5 m)
Impulse	Pelton Turgo	Cross-flow Turgo Multi-Jet Pelton	Cross-flow Multi-Jet Pelton	Water wheel
Reaction	-	Francis Pump-as-turbine	Propeller Kaplan	Propeller Kaplan

The 'capacity factor' is a ratio summarizing how hard a turbine is working, expressed as follows:

$$capacity\ \ factor\ (\%) = \frac{energy\ \ generated\ \ per\ year\ (kWH/\ year)}{installed\ \ capacity\ \ (kW)\cdot 8760\ \ hours/\ year} \tag{2}$$ [3]

Generators convert the mechanical (rotational) energy produced by the turbine to electrical energy. There are two types of generators: synchronous and asynchronous. Synchronous generators are standard in electrical power generation and are used in most power plants. Asynchronous generators are more commonly known as induction generators. Both of these generators are available in three-phase or single-phase systems. [2]

3. CASE STUDY AND RESULTS

The case study is for a mountain chalet - hotel with 30 rooms in a tourist area. The need for electrical energy is all over the year because the area has ski slopes in winter and rafting, climbing and other summer activities. The flow is from a real river but by economical reasons we can't provide the name and the location of it. The analyze is made using RETScreen software which is a decision support tool developed with the contribution of numerous experts from Canadian government, industry, and academia. The software can be used to evaluate the energy production and savings, costs, emission reductions, financial viability and risk for various types of renewable energy.

The hydropower system is connected to central grid (20 kW) witch is located nearby. We chose to have backup batteries so we use synchronous generators and an inverter. We have made a list of consumers resulting the electrical power necessary for the building, the installed power P_i=70 kW.

The water intake location was chosen at the limit with the protected area so that we can obtain all the necessary approvals, the type of water intake is Tyrolean. The location where the power house will be located belongs to the owner of the mountain chalet – hotel. The distance between the intake and the power house is 2500 m resulting a head of 100 m. The connection between intake and power house will be made with an PAFSIN GRP adduction, with diameter D=600 mm and asperity e=0,03 mm. In calculating the diameter of the adduction the maximum hydraulic losses was considered 6,6%.

Knowing the head (100 m) and the design flow (0,430 m^3/s) we have chosen from product database a single impulse turbine, Pelton model, manufactured by Voith Siemens. (Fig. 2)

Resource assessment		
Proposed project		Run-of-river
Hydrology method		User-defined
Gross head	m	100,0
Maximum tailwater effect	m	0,00
Residual flow	m³/s	0,091
Percent time firm flow available	%	55,0%
Firm flow	m³/s	0,44
Hydro turbine		
Design flow	m³/s	0,430
Type		Pelton
Turbine efficiency		Standard
Number of jets for impulse turbine	jet	6
Number of turbines		1
Manufacturer		Voith Siemens
Model		Pelton
Efficiency adjustment	%	0,0%
Turbine peak efficiency	%	83,6%
Flow at peak efficiency	m³/s	0,3
Turbine efficiency at design flow	%	83,2%

Fig. 2 – Inserted data and results from RETScreen

After inserting the flow values in the program according to the hydro data achieved from Hydrological Institute (table 2), we obtained the following turbine efficiency curve (Fig. 3) and flow duration and power curves (Fig. 4) for that specific river. The firm flow (0.44 m^3/s) was calculated by the software after inserting the hydrological data and residual flow (0,091 m^3/s).

Table 2. Hydrological data and results for turbine efficiency and combine efficience

%	Flow m³/s		Turbine efficiency	Number of turbines	Combined efficiency
0%	10,00		0,00	0	0,00
5%	5,30		0,18	1	0,18
10%	3,68		0,50	1	0,50
15%	2,95		0,68	1	0,68
20%	2,51		0,77	1	0,77
25%	2,14		0,81	1	0,81
30%	1,85		0,83	1	0,83
35%	1,65		0,83	1	0,83
40%	1,51		0,84	1	0,84
45%	1,37		0,84	1	0,84
50%	1,26		0,84	1	0,84
55%	1,18		0,84	1	0,84
60%	1,11		0,84	1	0,84
65%	1,04		0,84	1	0,84
70%	0,98		0,84	1	0,84
75%	0,92		0,84	1	0,84
80%	0,88		0,84	1	0,84
85%	0,83		0,84	1	0,84
90%	0,75		0,84	1	0,84
95%	0,68		0,84	1	0,84
100%	0,40		0,83	1	0,83

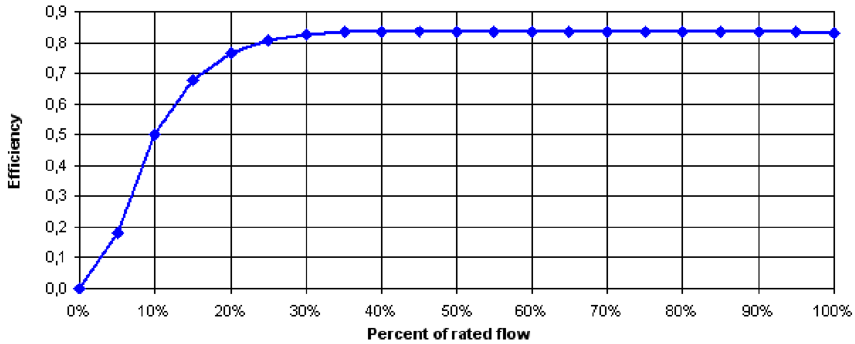

Fig. 3 – Turbine efficiency

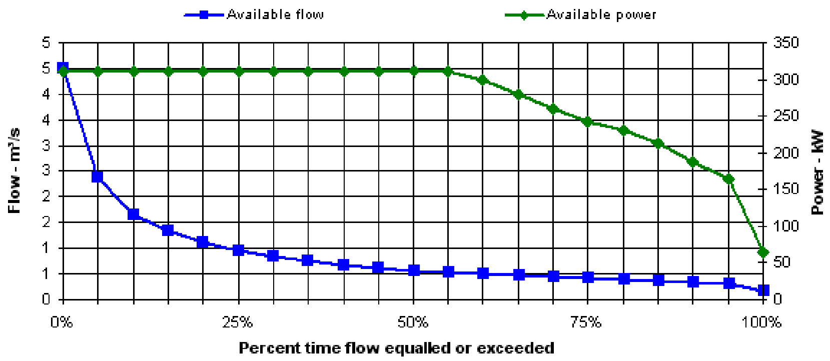

Fig. 4 – Flow duration and power curves

As it can be seen from the graph the turbine peak efficiency is 83,6% at a flow of 0,3 m^3/h. The generator efficiency is 95% and capacity factor is 88,2%. The power capacity resulted is 311 kW. The difference between the value obtained and the power needed for the hotel (approximately 240 kW) will be injected to the central grid. Considering that the area where the hydropower plant will be build is in continuous development, the extra energy witch is injected in the central grid, in the future, can be sold to other investors nearby.

The program also calculates the greenhouse gas (GHG) emission reduction witch was obtained with construction of this hydropower system. The net annual GHG emission reduction is equivalent with 1149 tCO_2.

The software estimate that the investment will be recovered in approximately 3 years for a project estimated life of 30 years (fig. 4).

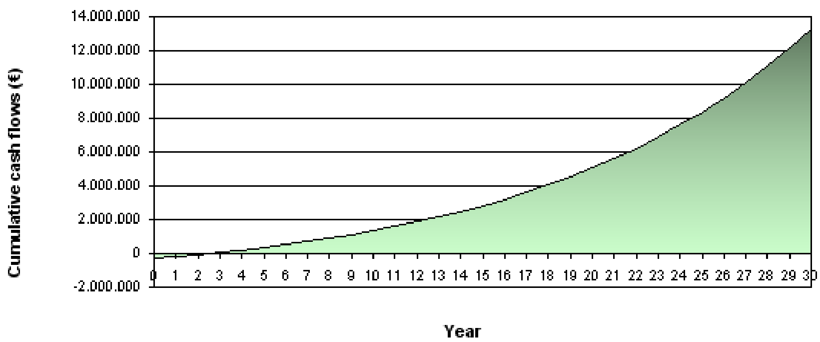

Fig. 4 – Cumulative cash flows graph

4. CONCLUSIONS

We have chosen an optimal positioning of the intake and power plant to obtain a maximum head. The Tyrolean intake is located on the main river, in the most concentrated area in terms of affluent rivers so we can take a higher flow, outside the protected area.

The optimal diameter for the adduction was chose for not having higher hydraulic losses. By using the PAFSIN GRP material for adduction because it has smaller asperity, we obtained a diameter of 600 mm, comparing with a steel adduction witch would be with 100 mm bigger.

The design flow was chosen smaller than the firm flow resulting a constant function of turbine during the entire year, considering that the river flow is variable and it also ensures the power needed for the mountain chalet – hotel. Even more, it provides profit by injecting the remaining power into the central grid.

The turbine will operate at maximal parameters about 60% of the year according to the graphics obtained through the RETScreen software.

Electricity production from hydropower has been, and still is today, the first renewable source used to generate electricity. Nowadays hydropower electricity in the European Union both large and small scale represents 13% of the total electricity generated, so reducing the CO2 emissions by more than 67 million tons a year.

The most important advantages that hydropower systems have over wind, wave and solar power are:

• a high efficiency (70 - 90%), by far the best of all energy technologies;
• a high capacity factor (typically >50%), compared with 10% for solar and 30% for wind;
• a high level of predictability, varying with annual rainfall patterns;
• slow rate of change; the output power varies only gradually from day to day (not from minute to minute);
• a good correlation with demand i.e. output is maximum in winter;
• it is a long-lasting and robust technology; systems can readily be engineered to last for 50 years or more.

RETScreen is a very useful tool for verifying technical and economical aspects for a hydropower system. Using this software we were able obtain information that this hydropower system can provide the necessary power needed for the hotel and also an estimated period for recover the initial investment.

REFERENCES

[1] Natural Resources Canada, *Small hydro project analysis chapter*, Canada 2004

[2] Natural Resources Canada, *Micro-Hydropower systems*, Canada, 2004

[3] The British Hydropower Association, *A guide to UK mini-hydro developments*, UK, 2005

[4] Y. Aslana, O. Arslanb, C. Yasara, *A sensitivity analysis for the design of small-scale hydropower plant: Kayabogazi case study*, Renewable energy, volume 33, pp. 791-801, 2007

[5] R. Bakis, *Electricity production opportunities from multipurpose dams (case study)*, Renewable energy, volume 32, pp. 1723-1738, 2007

[6] K. V. Alexander, E. P. Giddens, *Microhydro: Cost-effective, modular systems for low heads*, Renewable energy, volume 33, pp. 1379-1391, 2008

[7] A. A. Williams, R. Simpson, *Pico hydro – Reducing technical risks for rural electrification*, Renewable energy, volume 34, pp. 1986-1991, 2009

[8] U.S.A. National Renewable Energy Laboratory, *Small hydropower systems*, USA, 2001

[9] G. Taljan, A.F. Gubina, *Energy-based system well-being analysis for small systems with intermittent renewable energy sources*, Renewable energy, volume 34, pp. 2651-2661, 2009

[10] European Small Hydropower Association, *Guide on how to develop a small hydropower plant*, 2004

[11] H. Ramos, B. A. de Almeida, *Small hydropower schemes as an important renewable energy source*, International Conference Hidroenergia (99), Vienna, Austria, 1999

[12] http://www.retscreen.net/

INSTRUCTIONS FOR AUTHORS

Name **SURNAME**, Name **Surname, ...**
Affiliation, email of 1st author, Affiliation, email of 2nd author, ...

Key words: List 3-4 keywords
Abstract*: Abstract of max. 120 words*

1. INTRODUCTION

The paper must be written in English. It shall contain at least the following chapters: Introduction, research course (mathematical algorithm); method used; results and conclusions, references.

Use DIN A4 Format (297 x 210 mm) MSWord format. Margins: top, bottom, left and right 2.5 mm each. The text should be written on one side of the page only. Use Times New Roman fonts, line spacing 1. The font formats are: paper title: 14 pt bold italic, capital letters, author's name(s): 12 pt italic for name and 12 pt. bold, italic for surname; Affiliation: 11 pt. italic; key words: 10 pt, bold; Abstract: 10 pt. italic, word Abstract in 10 pt. bold; chapter titles (do not use automatic numbering): 12 pt bold, capital letters; subtitles: 12 pt bold lower capitals; body text: 12 pt. regular. tables and figures caption: 11 pt. italic; references: author 11 pt. bold, title 11 pt. italic, year, pages, ... in regular.

The number of pages is not restricted.

2. FIGURES AND TABLES

Figures have to be made in high quality, which is suitable for reproduction and print. Don't include photos or color prints. Place figures and tables at the top or bottom of a page wherever possible, as close as possible to the first reference to them in the paper.

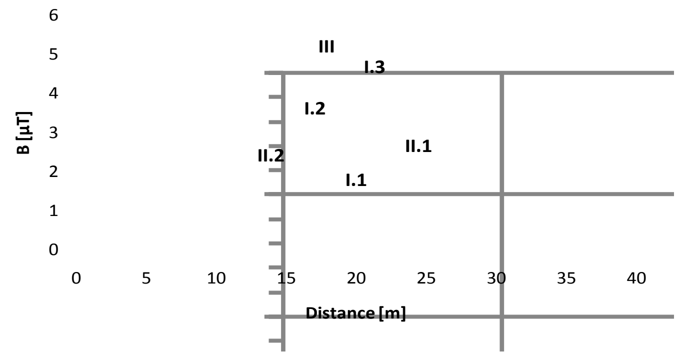

Fig. 4 - Magnetic flux density at 1 m above the ground

Table1. Transposing principle

	Circuit											
	1	*2*	*1*	*2*	*1*	*2*	*1*	*2*	*1*	*2*	***1***	***2***
1/3	*R*	*T*	***R***	***R***	*R*	*S*	*R*	*T*	*R*	*S*	***R***	***R***
line	***S***	***S***	*S*	*T*	*S*	*R*	*S*	*R*	*S*	*T*	***S***	***S***
length	*T*	*R*	*T*	*S*	***T***	***T***	*T*	*S*	*T*	*R*	***T***	***T***
1/3	*T*	*S*	***T***	***T***	*T*	*R*	*T*	*S*	*T*	*R*	***T***	***T***
line	***R***	***R***	*R*	*S*	*R*	*T*	*R*	*T*	*R*	*S*	***R***	***R***
length	*S*	*T*	*S*	*R*	***S***	***S***	*S*	*R*	*S*	*T*	***S***	***S***
1/3	*S*	*R*	***S***	***S***	*S*	*T*	*S*	*R*	*S*	*T*	***S***	***S***
line	***T***	***T***	*T*	*S*	*T*	*S*	*T*	*S*	*T*	*R*	***T***	***T***
length	*R*	*S*	*R*	*T*	***R***	***R***	*R*	*T*	*R*	*S*	***R***	***R***
Name	***I.1***		***I.2***		***I.3***		***II.1***		***II.2***		***III***	

3. EQUATIONS

Equations are centred on page and are numbered in round parentheses, flush to right margin. In text respect the following rules: all variables are italic, constants are regular; the references are cited in the text between right parentheses: [1], the list of references has to be arranged in order of citation.

REFERENCES

1. International Commission on Non-ionizing Radiation Protection, *Guidelines for limiting exposure to time-varying electric, magnetic and electromagnetic fields (Up to 300 GHz)*, Health Physics, **74**, pp. 494-522, 1998.

2. A. Marincu, M. Greconici, *The electromagnetic field around a high voltage 110 KV electrical overhead lines and the influence on the biological sistems,* Proceedings of the 5th International Power Systems Conference, pp. 357-362, Timisoara, 2003.

3. Gh. Hortopan, *Compatibilitate electromagnetică,* Ed. Tehnică, 2005.